R. & M. No. 2912
(13,123)
A.R.C. Technical Report

MINISTRY OF SUPPLY

AERONAUTICAL RESEARCH COUNCIL
REPORTS AND MEMORANDA

Choking Effects and some Reynolds Number Effects on the Mach Number Distribution round a Two-dimensional Aerofoil in the RAE 10-ft x 7-ft High-Speed Tunnel

By

D. A. CLARKE, B.Sc. (Eng.), A.C.G.I., and H. E. GAMBLE, B.Sc.

LONDON: HER MAJESTY'S STATIONERY OFFICE
1955
EIGHT SHILLINGS NET

Choking Effects and some Reynolds Number Effects on the Mach Number Distribution round a Two-dimensional Aerofoil in the RAE 10-ft x 7-ft High-Speed Tunnel

By

D. A. CLARKE, B.Sc.(Eng.), A.C.G.I., and H. E. GAMBLE, B.Sc.

COMMUNICATED BY THE PRINCIPAL DIRECTOR OF SCIENTIFIC RESEARCH (AIR), MINISTRY OF SUPPLY

*Reports and Memoranda No. 2912**
September, 1949

Summary.—A two-dimensional aerofoil of NACA 0015 section was tested at zero incidence in the Royal Aircraft Establishment 10 ft × 7 ft High-Speed Wind Tunnel and measurements were made of

(*a*) Static pressure on the aerofoil surface at Reynolds numbers of $1{\cdot}4 \times 10^6$ to $5{\cdot}5 \times 10^6$

(*b*) Static pressure on the aerofoil surface, on the tunnel walls and in the stream between the aerofoil and the walls at $R = 2{\cdot}8 \times 10^6$.

All the tests were made at Mach numbers of 0·7 upwards and were continued past the choking Mach number of 0·764 until either the maximum permissible fan speed was reached or the maximum available power was being used.

The results showed that the choking Mach number was about 0·764 at Reynolds numbers from $1{\cdot}4 \times 10^6$ to $2{\cdot}8 \times 10^6$. Above $M = 0{\cdot}760$ the development of the supersonic region towards the walls was extremely rapid in terms of tunnel Mach number. At $M = 0{\cdot}761$ the sonic line was only about half-way out to the tunnel walls and at $M = 0{\cdot}764$ it had reached them.

Before and during choking quite large changes in the aerofoil pressure distributions were produced by varying the Reynolds number. At $M = 0{\cdot}73$ and 0·75 the shape of the pressure distribution curves indicated the possibility of a λ-shock at the lower Reynolds numbers and a single shock at the higher Reynolds numbers.

1. *Introduction.*—Tests were made in May, 1947 in the R.A.E. 10 ft × 7 ft High-Speed Wind Tunnel to investigate the effect of Reynolds number on aerofoil pressure distribution at high subsonic Mach numbers and to obtain information on the phenomenon of choking (see section 2 for definitions).

A large aerofoil was chosen, so that when the choking Mach number was first reached there would still be large reserves of power and fan speed available for examining the further development of the supersonic region.

2. *Definition of Choking Mach Number.*—The tunnel Mach number is obtained from pressure measurements at two reference holes upstream of the working-section. It is the mean Mach number at the working-section when there is no model present.

As the fan speed is increased the tunnel Mach number does not increase indefinitely but reaches a limiting value at which it remains almost constant. This value is known as the choking Mach number and depends on the relative size of the model and tunnel. The reason for this limit to the

* R.A.E. Report Aero. 2337, received 8th May, 1950.

tunnel Mach number can be briefly explained as follows. Before the tunnel chokes, increasing the fan speed, and hence increasing the tunnel Mach number, causes an extension of the supersonic region around the aerofoil both outwards from the surface and downstream. When supersonic flow extends from the model to the tunnel walls, increasing the fan speed can affect the upstream conditions only through the subsonic parts of the boundary layers. (In a return-flow tunnel it may also change the general pressure level, but this has no effect on the Mach number distribution.) Thus when the supersonic region stretches right across the tunnel the Mach number measured upstream of the model has reached its maximum attainable value. The only effect of decreasing the downstream pressure, by increasing the fan speed, is to extend the supersonic region further downstream.

3. *Experimental Details.*—A full description of the tunnel is given by Thompson[1]. Before the present tests additional small fillets had been inserted in the corners of the working-section to improve the longitudinal velocity distribution.

The rig is shown in Figs. 1, 2 and 3. A 37·5-in. chord NACA 0015 aerofoil spanned the tunnel vertically and was set at zero incidence. During the tests without the static-comb the aerofoil was braced by two 10-cwt cables on each side, but these were removed for the rest of the tests. The aerofoil was made of laminated teak and had a smooth polished 'Phenoglaze' finish. Details of the section and the position of the pressure holes are given in Tables 1 and 2.

Static pressures between the aerofoil and the walls were measured by means of a comb of ten tubes, *see* Figs. 1 and 2. The arrangement of the static-holes and the shape of the nose of each tube, Fig. 4, were identical with those used in all high-speed tunnel calibrations, the holes being 12·4 diameters behind the nose.

At the rear the tubes were supported by a strut of about 1-ft chord and 15 per cent thick, spanning the tunnel horizontally and placed sufficiently far downstream to avoid large interferences in the field of the aerofoil. This supporting strut was braced by cables anchored to plates on the tunnel floor and roof.

Towards the front the tubes were braced vertically by 20-gauge wires and also, at the same points, by a horizontal wire of the same gauge stretching right across the tunnel. In some cases it was necessary to anchor this wire to a steel strap placed across the window.

The positions of the comb static-holes were varied by large amounts by movement of the supporting strut and by small amounts up to 7 in. by inserting different lengths of sleeve at A, Fig. 2.

Notes on the position and the rig for each case tested are given in Tables 3 and 5. The positions of the pressure holes in the side walls are given in Table 4 and Fig. 3.

The expressions 'near side' and 'far side' refer respectively to the surfaces of the aerofoil nearest to and farthest from the tunnel operator, *i.e.*, in plan view, looking upstream, the port and starboard sides of the tunnel.

4. *Range of Tests.*—The tests were made at tunnel Mach numbers of 0·70 and above. Before inserting the static-comb, pressures were measured on the walls and on the aerofoil at five different Reynolds numbers. The highest of these ($R = 5{\cdot}5 \times 10^6$) was chosen to give a Mach number of 0·70 at the maximum power available (3400kW). The lowest ($R = 1{\cdot}4 \times 10^6$) was determined by the lowest tunnel pressure that could conveniently be obtained by the suction pumps (about 2·5 in. Hg). The limits to the maximum development of the supersonic region were fixed at the lower Reynolds numbers by the maximum speed at which the fan could be run (850 r.p.m.), and at the higher Reynolds numbers by the maximum power available. These limits are illustrated in Fig. 5. From this figure it can be seen that the maximum Reynolds number at which choking could usefully be investigated up to full fan speed was about $R = 2{\cdot}8 \times 10^6$. Accordingly the static-comb measurements were made at this Reynolds number.

Static pressures on the aerofoil, on the walls and in the stream were measured for seven positions of the comb static-holes between 45 and 97 per cent of the aerofoil chord back from the leading edge (*see* Table 5), for Mach numbers of 0·70, 0·72, 0·74, 0·75 and then at intervals of 10 r.p.m. up to 850 r.p.m. No static-tube pressures are available above $M = 0{\cdot}760$ for case B_3 (*see* Table 5) because of a failure of the camera photographing the manometer board.

5. *Analysis of Readings.*—All values of static pressure p have been calculated as fractions of H_0, the mean total head in the working-section. In some of the figures, these values of p/H_0 have been translated into local Mach number and it has been assumed for this purpose that there is no loss of total head through the shock. If the shock is normal the theoretical loss of total head through it for the worst condition considered, *i.e.*, when the Mach number ahead of the shock is at its maximum value of 1·37, is about 3·6 per cent. Thus, for this extreme case, Mach numbers behind the shock quoted as 0·8 and 0·9 are really about 0·76 and 0·87 respectively.

Whereas before choking, the tunnel Mach number is a satisfactory parameter by which to compare pressure distributions, it cannot of course be used when the tunnel is choked. After the tunnel choked, it was found that a steady increase in fan speed caused a steady increase in the local Mach number (or decrease in p/H_0) over the rear part of the aerofoil. Accordingly, the mean value of p/H_0 over a suitable portion of the aerofoil was taken as the standard of reference. For the tests on the aerofoil alone there were changes in pressure distribution with Reynolds number over most of the surface. Therefore the mean p/H_0 used for comparing these tests was found for each surface of the aerofoil by taking the average of the pressures at all holes on that surface including the trailing-edge hole. For the tests with the static-comb present for which the Reynolds number was constant, changes in distribution are only due to backward movement of the shock wave and mainly occur aft of 50 per cent of the chord. Thus in these cases a mean p/H_0 was found for each surface, by taking the average of the pressures at all holes on the rear half of that surface including the 50 per cent hole and the trailing-edge hole. The relationships between tunnel Mach number and the above parameters are given in Table 6 and shown in Figs. 12a and 12b.

6. *Effect of Rig on Tests.*—The fan speed (and power) required to obtain any particular pressure distribution or position of the shock on the aerofoil was greatly increased by the presence of the static-comb and supporting strut. (Figs. 14 and 20.) Forward movement of the comb supporting strut further increased the fan speed required for any particular aerofoil distribution. Also, the position of the shock on the aerofoil surface when the sonic line just reached the tunnel wall was $0{\cdot}04c$ further aft when the static-comb was in position. (Fig. 20.)

These conditions meant that even for the maximum fan speed (850 r.p.m.) the sonic line did not reach the wall when the comb supporting strut was in the forward position and only just reached it (at 840 r.p.m.) when the comb strut was further back. (Figs. 14 and 20.)

From comparisons at constant mean p/H_0 of the pressures on the aerofoil surface and on the walls it appears that movement of the static-comb had little effect on the shape of the pressure distributions. Small differences, which occur in the aerofoil pressure distributions, cannot be correlated with the position of the static-comb and are probably mainly due to a slight warping of the aerofoil during the course of the tests. It may be mentioned here that the conditions under which the tests were made were rather severe for a wooden aerofoil. Most of the tests were run at a tunnel stagnation temperature of about 45 deg C.

The presence of the strap across the window (*see* Table 5) caused some distortion of the nearby wall pressures. It is hoped that this effect did not extend into the stream as far as the static-comb and where wall pressures have been used they have been taken from those cases without the strap.

The static-comb was not calibrated but a test was made with the comb in position in the otherwise empty tunnel. All the tubes read the same pressure, within the accuracy of measurement, up to a Mach number of 0·8 above which no readings were taken.

It is not expected that local shock and boundary-layer effects near the nose of the tubes influenced the pressures at the holes. It is possible that, in supersonic flow, the bow-wave from the front of one tube may have affected the pressures as measured on an adjacent tube or on the aerofoil surface. It is also probable that the boundary layers on the tubes had some effect on the measured pressures when a shock in the tunnel stream was near the measuring holes on the static-tubes. In this case the pressure gradient apparent through the shock-wave may be dependent on the comb interference. This does not seriously affect the graphs shown in this report.

7. *Results and Discussion.*—7.1. *Reynolds Number Effects up to* $M = 0{\cdot}75$.—Figs. 7a to 7d show the measured pressure distributions on the aerofoil for four different Reynolds numbers, and in Figs. 10a, 10b and 10c distributions for various Reynolds numbers are compared at constant Mach number.

At a Mach number of $0{\cdot}70$ (Fig. 10a) the velocity is supersonic for about 15 per cent of the chord just before the maximum thickness. This is followed by a small compression which can be attributed to a weak shock or perhaps to a succession of weak shocks. As drawn, Fig. 10a shows a greater rate of compression at the higher Reynolds numbers, but it must be remembered that the only pressure holes in this region are at 20, 30 and 37 per cent of the chord.

As the Mach number is increased the supersonic region grows and the compression occurs further back, while the size and rate of compression both increase.

At a Mach number of $0{\cdot}75$ (Fig. 10c) there are quite large differences in pressure distribution in the supersonic region for the different Reynolds numbers. At $R = 1{\cdot}38 \times 10^6$ the peak suction occurs at 30 per cent of the chord and is followed by a slow increase of pressure until the main compression which takes place at 50 per cent. At $R = 2{\cdot}98 \times 10^6$ the suction again reaches its maximum at 30 per cent, but now maintains this value until the main compression. At $R = 4{\cdot}89 \times 10^6$ the distribution flattens at 30 per cent, but at 35 per cent there is a further rise in suction to the peak value at 45 per cent. There is little difference in the form or position of the main compression for these three Reynolds numbers. At this Mach number of $0{\cdot}75$ the changes in surface distribution are confined to the region between 35 per cent and 65 per cent of the chord.

At the higher Reynolds numbers an expansion was sometimes observed at the surface, behind the main compression. In Fig. 7c for example, at a Mach number of $0{\cdot}720$ there is a rise of suction from the 37 per cent hole to the 43 per cent hole. A small kink in the distribution behind the main compression (*e.g.*, Fig. 7d, 782 r.p.m.) may well be evidence of an expansion further out in the stream. At the lower Reynolds numbers there was no evidence of such an expansion.

In the present tests it was not possible to measure the flow optically or to obtain detailed information about the boundary layer. However, the Reynolds number effects on the pressure distributions are similar to those obtained by other investigators who have been able to supplement their measurements by schlieren photographs[2,3]. Their results will, therefore, be used to help explain the changes with Reynolds number in the present tests.

7.2. *Results of Other Tests.*—By surface pressure measurements on a curved plate, by static and pitot traverses and by schlieren observation Ackeret[2] investigated the relation between the state of the boundary layer and the form of the shock system. Those of his results which are relevant here are given below.

(*a*) With a turbulent boundary layer there was a single shock almost normal to the surface and this produced the main compression at the surface. The peak suction at the surface occurred just before the shock. (This corresponds to the distribution at $M = 0{\cdot}73$, $R = 4{\cdot}84 \times 10^6$ in Fig. 10b.)

(*b*) With a laminar boundary layer a surface distribution was obtained similar to that in Fig. 10c at $R = 1{\cdot}38 \times 10^6$, $M = 0{\cdot}75$. In Ackeret's tests a λ-shock occurred with its main (aft) branch producing the main surface compression. Its oblique branch met the

surface at the point of peak suction and produced a slight fall in Mach number although the flow remained supersonic.

(*c*) Measuring from a point some way ahead of the main shock to one some way behind it, the boundary-layer momentum thickness increased by 5 times with a turbulent layer and by 10 times with a laminar layer. Reversed flow at the base of the main shock occurred only with a laminar layer.

Liepmann[3], has made observations by schlieren and surface pressure measurements on the flow over a circular profile. He found a similar relation between the state of the boundary layer and the form of the shock system.

In the present tests the pressure distributions at high Reynolds numbers (e.g., $R \geqslant 2{\cdot}8 \times 10^6$) are similar in shape to those obtained by Ackeret and by Liepmann when there was a single shock. Similarly, the low Reynolds number distributions correspond to those obtained with a laminar boundary layer and a λ-shock.

7.3. *Reynolds Number Effects Above* $M = 0{\cdot}75$.—Above a Mach number of $0{\cdot}75$ the increments in M for each increment in fan speed become progressively smaller until the choking Mach number is reached at $M = 0{\cdot}764$. The shock, however, continues to move back steadily, although the surface pressure gradient at its base now becomes smaller. At the lower Reynolds number this gradient defined as $d(p/H_0)/d\ (x/c)$ may fall from $2\frac{1}{2}$ at $M = 0{\cdot}75$ to as low as 1 when the shock is near the trailing edge.

Comparisons have been made at constant mean p/H_0 taken over the whole surface and these show the variations in the shape of the pressure distributions at different Reynolds numbers. Fig. 11a to 11e shows that the effect of increasing the Mach number is still to increase the suction immediately before the main shock. With the shock very far back the peak suction occurs at about 60 per cent of the chord at all Reynolds numbers.

7.4. *Choking.*—7.4.1. *The development of choking.*—Figs. 15a, 15b and 15c show typical static-pressure distributions across the tunnel as choking proceeds. In Figs. 17a to 17f the distributions are given in the form of isobars. It should be noted again that the local Mach numbers behind the shock are based on the assumption that there is no loss of total head through the shock. The gradients through the shock are smaller than would be expected from theory and this may perhaps be attributed to the presence of the boundary layers on the tubes, although it is possible that a small part may be due to temporal fluctuations of the shock position. The expansion behind the shock shown on the aerofoil pressure distributions did not extend as far out as the first tube and so does not appear on the graphs. The small differences, which develop at choking, between the pressures on the two sides of the aerofoil may be due to some lack of symmetry in the model or in its setting in the tunnel or in the direction of the flow. It cannot be attributed to the presence of the static-comb (*see* Fig. 13).

The spread of the supersonic region across the tunnel is shown in three different ways in Figs. 18, 19a, 19b. The extension of the supersonic region through the outer half of the stream is extremely rapid in terms of tunnel Mach number (Fig. 18). When the tunnel Mach number is only $0{\cdot}003$ below its choking value the shock has still extended over only the inner half of the stream.

7.4.2. *The value of the choking Mach number.*—The choking Mach number was $0{\cdot}764$ and was the same, within the accuracy of measurement ($\pm\ 0{\cdot}001$) at all Reynolds numbers tested. One-dimensional theory of flow gives a value of $0{\cdot}766$ from the equation

$$\frac{A_0}{A_0 - F} = \frac{1}{M}\left\{\frac{5 + M^2}{6}\right\}^3,$$

where A_0 is the cross-sectional area of the tunnel and F is the net frontal area of the model at its

greatest section. An allowance for a boundary layer on the tunnel walls of $\frac{3}{8}$-in. displacement thickness will reduce this value by about 0·001.

A possible explanation of the surprisingly close agreement between the choking Mach number as calculated from the crude one-dimensional theory and that measured in the tunnel is as follows. The theory assumes a sonic line straight across the tunnel at the point of maximum thickness of the aerofoil. This gives the maximum possible value of the mass flow. A typical Mach number distribution across the choked tunnel in this plane is given in Fig. 21, together with the mass flow distribution $\rho_v/\rho_T v_T$, where the suffix T indicates values at $M = 1$. The mean mass flow in this case is 0·993, which is very near the theoretical value of unity, in spite of the large variation of Mach number across the tunnel. Thus the estimated choking Mach number is not seriously in error.

8. *Conclusions.*—A two-dimensional NACA 0015 aerofoil, which had a chord of 0·32 times the tunnel breadth and spanned the tunnel vertically gave a choking Mach number of 0·764 at Reynolds numbers from $1{\cdot}4 \times 10^6$ to $2{\cdot}8 \times 10^6$.

The position of the sonic line in the stream was determined for various pressure distributions on the aerofoil surface as the tunnel choked. When the sonic line extended halfway out from the aerofoil to the tunnel walls the tunnel Mach number was only about 0·003 below its choking value.

At speeds below choking there were quite large changes with Reynolds number in the pressure distribution on the aerofoil surface. In general the effect of increasing the Reynolds number from $R \simeq 1{\cdot}3 \times 10^6$ to $R \simeq 5 \times 10^6$ was to increase the suction just ahead of the main shock.

By comparison with results of other investigators it appears that the shape of the pressure distribution at low Reynolds numbers (about 1×10^6) indicates the presence of a laminar boundary layer and a λ-shock. At higher Reynolds numbers the pressure recovery occurs through a single shock.

REFERENCES

No.	*Author*	*Title, etc.*
1	Staffs of the High-Speed Tunnel and High-Speed Flight Sections, R.A.E. Edited by W. A. Mair.	Research on high-speed aerodynamics at the Royal Aircraft Establishment from 1942 to 1945. R. & M. 2222. September, 1945.
2	J. Ackeret, F. Feldmann and N. Rott.	Investigations on compression shocks and boundary layers in fast-moving gases. Institute for Aerodynamics, E.T.H. Zürich. No. 10. 1946. A.R.C. 10,044. September, 1946.
3	H. W. Leipmann	The interaction between boundary layer and shock-waves in transonic flow. *J. Aero Sci.*, Vol. 13, No. 12. December, 1946.

TABLE 1

Ordinates of NACA 0015 *Section*

$\frac{x}{c}$	$\frac{y}{c}$	$\frac{x}{c}$	$\frac{y}{c}$
0	0	0·3000	0·07500
0·0125	0·02367	0·4000	0·07252
0·0250	0·03268	0·5000	0·06615
0·0500	0·04443	0·6000	0·05703
0·0750	0·05249	0·7000	0·04579
0·1000	0·05852	0·8000	0·03278
0·1500	0·06680	0·9000	0·01809
0·2000	0·07170	0·9500	0·01008
0·2500	0·07424	1·0000	0·00157

Leading-edge radius = 0·0248.

TABLE 2

Position of Pressure Holes on Aerofoil (see Fig. 3)

Distance from leading edge	Line	Distance from leading edge	Line
0·015	a	0·560	c
0·030	c	0·600	a
0·050	d	0·650	d
0·080	b	0·690	b
0·140	c	0·730	d
0·200	b	0·780	a
0·300	c	0·820	c
0·370	d	0·880	d
0·430	b	0·950	b
0·500	a	1·000	d

The positions are the same on the two surfaces.

TABLE 3

Position of Comb Holes (Mean of all cases)

Far		Near	
Tube No.	Distance from tunnel centre-line (as fraction of aerofoil chord)	Tube No.	Distance from tunnel centre-line (as fraction of aerofoil chord)
5	0·241	6	0·236
4	0·429	7	0·422
3	0·643	8	0·635
2	0·963	9	0·955
1	1·283	10	1·275
Wall	1·596	Wall	1·604

TABLE 4

Position of Wall Holes (*see Fig.* 3)

(From leading edge of aerofoil, as a fraction of aerofoil chord, measured downstream)

Far		Near	
Distance	Line	Distance	Line
−0·978	B	−0·981	B
−0·658	B	−0·658	B
−0·338	B	−0·338	B
−0·018	C	−0·015	C
0·302	A	0·305	A
0·302	C	0·332	C
0·624	C	0·629	C
0·797	C	0·802	C
0·949	C	0·949	C
1·119	C	1·122	C
1·267	C	1·269	C
1·587	A	1·585	A
1·585	C	1·585	C
2·222	B		

TABLE 5

Details of Rig

Case	Mean distance back of comb holes from aerofoil leading edge	Mean distance back of noses from aerofoil leading edge	Distance of horizontal bracing wire from aerofoil trailing edge	Size of Sheath	Distance to leading edge of comb aerofoil from trailing edge of main aerofoil	Remarks
B1	0·779	0·666	0·433	Long	1·700	No bracing cables on main aerofoil in any of these cases
B2	0·965	0·832	0·434	Short	1·700	
B3	0·646	0·513	0·113	Short	1·380	Strap across port window
B5	0·458	0·325	0·110	Long	1·380	,, ,, ,, ,,
B5	0·805	0·672	0·277	Short	1·540	,, ,, ,, ,,
B6	0·711	0·578	0·273	Medium	1·540	,, ,, ,, ,,
B7	0·618	0·458	0·273	Long	1·540	,, ,, ,, ,,
C	As in Case B7, but with main aerofoil removed.					

TABLE 6

Test Data

Aerofoil + static-comb

R.P.M.	M	Reynolds number	Mean p/H over rear half of surface	
			Far	Near
		Case B1		
724	0·700	2·80	0·681	0·682
743	0·721	2·79	0·663	0·665
764	0·740	2·81	0·651	0·653
780	0·750	2·80	0·630	0·633
804	0·759	2·81	0·581	0·590
809	0·760	2·79	0·572	0·580
820	0·763	2·79	0·539	0·551
820	0·763	2·79	0·534	0·548
830	0·763	2·77	0·506	0·526
840	0·764	2·82	0·482	0·504
840	0·764	2·80	0·485	0·508
850	0·763	2·78	0·473	0·459
848	0·763	2·78	0·473	0·495
		Case B2		
723	0·700	2·83	0·681	0·681
742	0·719	2·81	0·665	0·667
765	0·740	2·79	0·651	0·652
784	0·751	2·79	0·625	0·628
810	0·760	2·78	0·566	0·577
820	0·762	2·77	0·542	0·556
830	0·763	2·78	0·516	0·536
839	0·764	2·81	0·492	0·515
850	0·764	2·80	0·471	0·490
		Case B3		
727	0·699	2·82	0·680	0·681
745	1·720	2·82	0·661	0·662
770	0·740	2·80	0·650	0·651
790	0·750	2·81	0·626	0·627
814	0·759	2·81	0·585	0·587
818	0·760	2·81	0·574	0·577
825	0·761	2·81	0·559	0·565
821	0·760	2·82	0·563	0·568
830	0·762	2·83	0·544	0·522
814	0·758	2·80	0·583	0·585
790	0·750	2·81	0·628	0·626

R.P.M.	M	Reynolds number	Mean p/H over rear half of surface	
			Far	Near
		Case B4		
731	0·700	2·81	0·679	0·679
735	0·710	2·81	0·671	0·672
744	0·720	2·82	0·662	0·663
753	0·729	2·81	0·654	0·656
766	0·740	2·82	0·649	0·650
788	0·750	2·80	0·625	0·626
814	0·759	2·80	0·577	0·579
820	0·761	2·80	0·562	0·566
830	0·763	2·80	0·543	0·550
840	0·763	2·80	0·517	0·5v1
850	0·764	2·80	0·496	0·513
		Case B5		
721	0·700	2·81	0·681	0·682
741	0·720	2·81	0·663	0·665
762	0·740	2·83	0·649	0·651
778	0·749	2·81	0·634	0·636
804	0·760	2·81	0·584	0·588
820	0·763	2·81	0·546	0·555
830	0·764	2·81	0·515	0·536
840	0·764	2·82	0·494	0·517
850	0·765	2·82	0·476	0·496
835	0·764	2·78	0·504	0·526
		Case B6		
726	0·700	2·79	0·680	0·681
745	0·720	2·80	0·663	0·665
763	0·740	2·82	0·648	0·650
781	0·750	2·82	0·629	0·632
805	0·760	2·82	0·582	0·587
820	0·763	2·81	0·547	0·556
825	0·763	2·82	0·535	0·549
830	0·763	2·82	0·524	0·542
840	0·764	2·82	0·498	0·519
850	0·765	2·83	0·478	0·499

R.P.M.	M	Reynolds number	Mean p/H over rear half of surface	
			Far	Near
		Case B7		
723	0·700	2·80	0·679	0·681
739	0·720	2·80	0·662	0·664
761	0·740	2·81	0·647	0·649
778	0·749	2·82	0·632	0·636
804	0·759	2·80	0·586	0·591
819_5	0·763	2·81	0·549	0·557
830	0·763	2·81	0·523	0·541
840	0·764	2·81	0·494	0·518
850	0·7645	2·82	0·478	0·505

TABLE 6—*continued*

Test Data

Aerofoil alone

R.P.M.	M	Reynolds number	Mean p/H over whole surface		Mean p/H over rear half of surface	
			Far	Near	Far	Near
699	0·700	2·81	0·638	0·638	0·680	0·681
711	0·720	2·83	0·619	0·618	0·663	0·664
729	0·740	2·79	0·593	0·592	0·650	0·651
743	0·751	2·81	0·571	0·571	0·632	0·625
761	0·759	2·83	0·543	0·545	0·578	0·5858
770	0·762	2·84	0·529	0·534	0·555	0·565
780	0·763	2·81	0·510	0·517	0·520	0·535
790	0·764	2·83	0·487	0·497	0·479	0·500
800	0·764	2·83	0·467	0·480	0·443	0·469
810	0·764	2·82	0·456	0·467	0·421	0·446
819_5	0·764	2·83	0·444	0·451	0·400	0·417
830	0·765	2·83	0·431	0·431	0·378	0·381
840	0·764	2·80	0·421	0·419	0·360	0·358
850	0·764	2·79	0·415	0·414	0·349	0·349

R.P.M.	M	Reynolds number	Mean p/H over whole surface
693	0·698	5·45	0·643
693	0·699	4·78	0·643
717	0·731	4·83	0·604
742	0·750	4·89	0·570
699	0·700	3·78	0·642
720	0·730	3·85	0·605
742	0·750	3·91	0·572
750	0·754	3·94	0·652
759_5	3·94	0·549	0·549
770	0·759	3·89	0·535
782	0·762	3·78	0·509
790	0·763	3·78	0·496
794	0·763	3·76	0·493
701	0·700	2·75	0·639
726	0·731	2·81	0·605
745	0·750	2·87	0·574
760	0·758	2·89	0·552
770	0·759	2·89	0·538
780	0·763	2·90	0·514
790	0·764	2·91	0·492
800	0·763	2·90	0·475
810	0·764	2·90	0·465
819	0·764	2·89	0·449
830	0·764	2·88	0·434
840	0·764	2·87	0·423

R.P.M.	M	Reynolds number	Mean p/H over whole surface
712	0·700	1·63	0·638
732	0·729	1·69	0·608
755	0·750	1·74	0·573
777	0·758	1·76	0·546
780	0·762	1·77	0·530
790	0·763	1·78	0·513
800	0·764	1·79	0·494
810	0·765	1·79	0·472
820	0·764	1·79	0·459
830	0·765	1·80	0·441
840	0·765	1·80	0·429
850	0·766	1·81	0·418
699	0·700	1·29	0·638
735	0·729	1·34	0·608
756	0·750	1·38	0·575
777	0·760	1·41	0·542
790	0·763	1·43	0·517
800	0·765	1·43	0·497
810	0·765	1·39	0·479
820	0·765	1·39	0·462
830	0·764	1·40	0·449
840	0·765	1·40	0·434
850	0·765	1·41	0·423

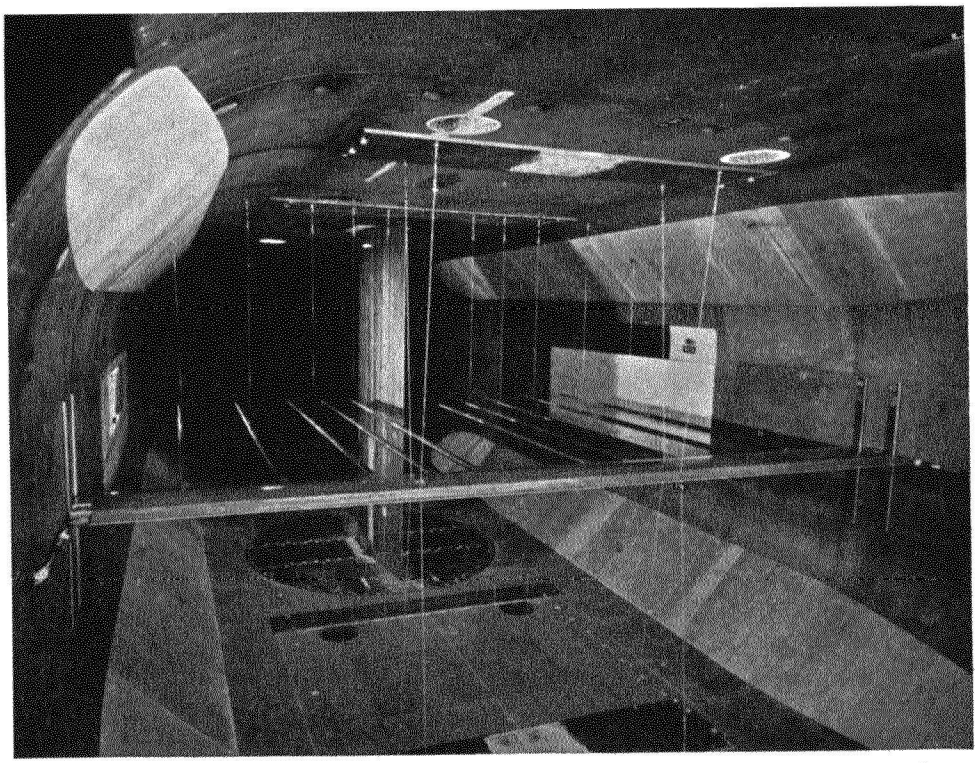

FIG. 1. Static-comb and NACA 0015 aerofoil in high-speed tunnel.

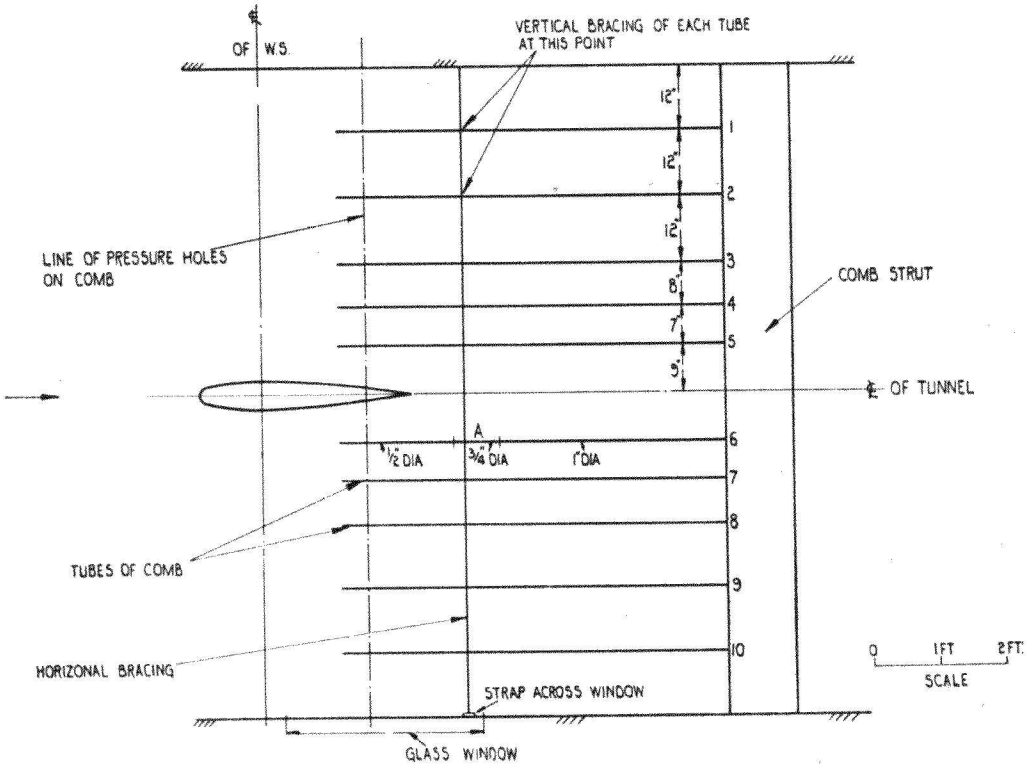

FIG. 2. Diagrammatic plan of rig for a typical case.

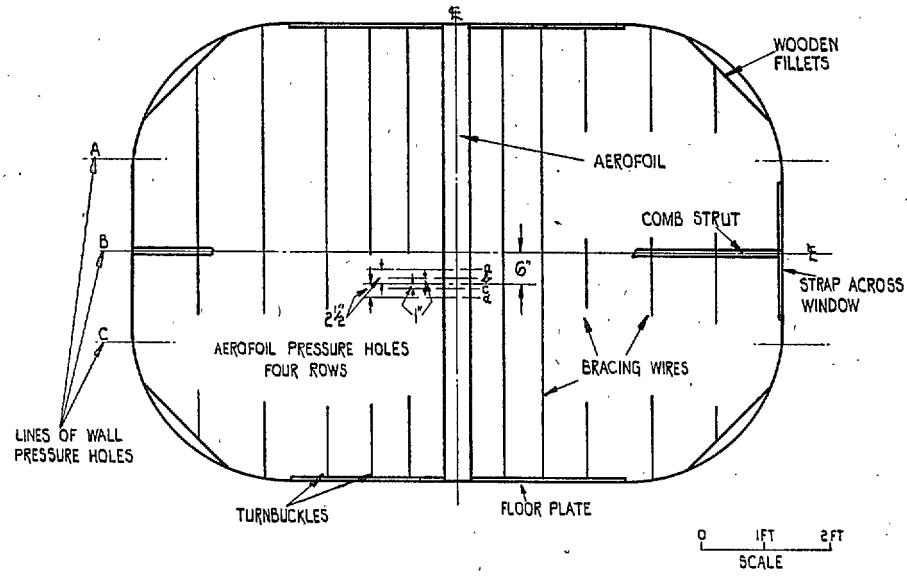

FIG. 3. Diagram at working-section.

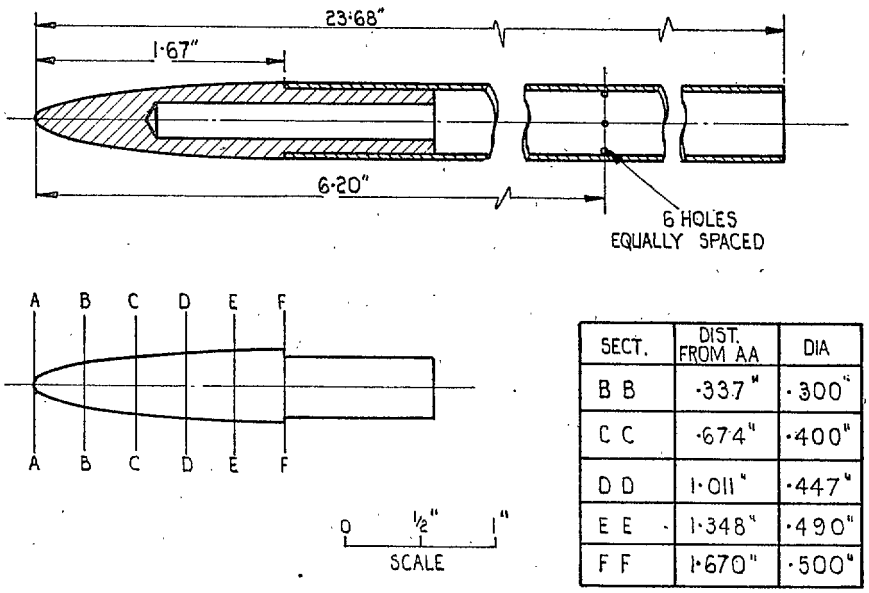

SECT.	DIST. FROM AA	DIA
B B	·337"	·300"
C C	·674"	·400"
D D	1·011"	·447"
E E	1·348"	·490"
F F	1·670"	·500"

FIG. 4. Details of nose of tubes.

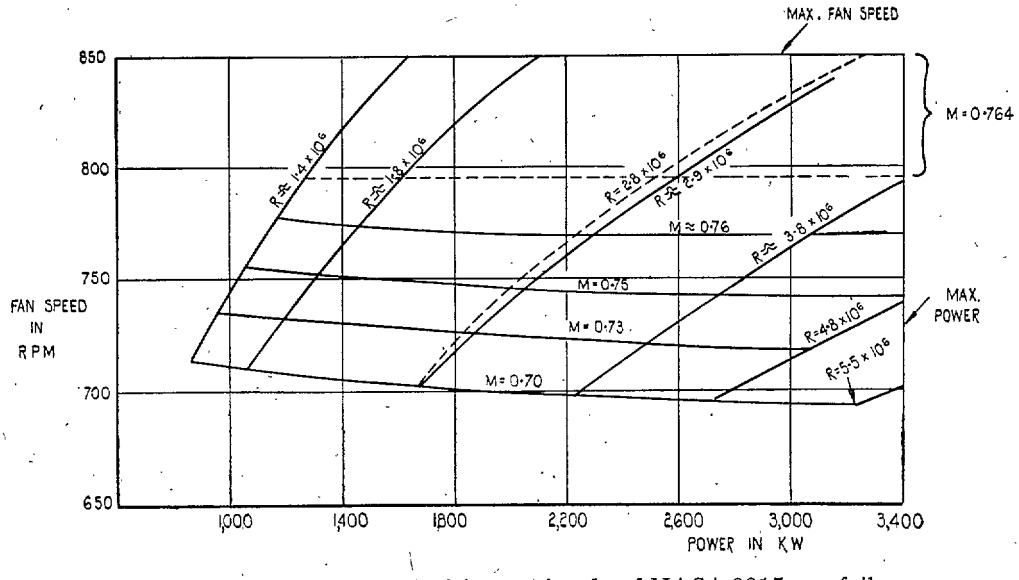

FIG. 5. Limits of tunnel with 37·5-in. chord NACA 0015 aerofoil.

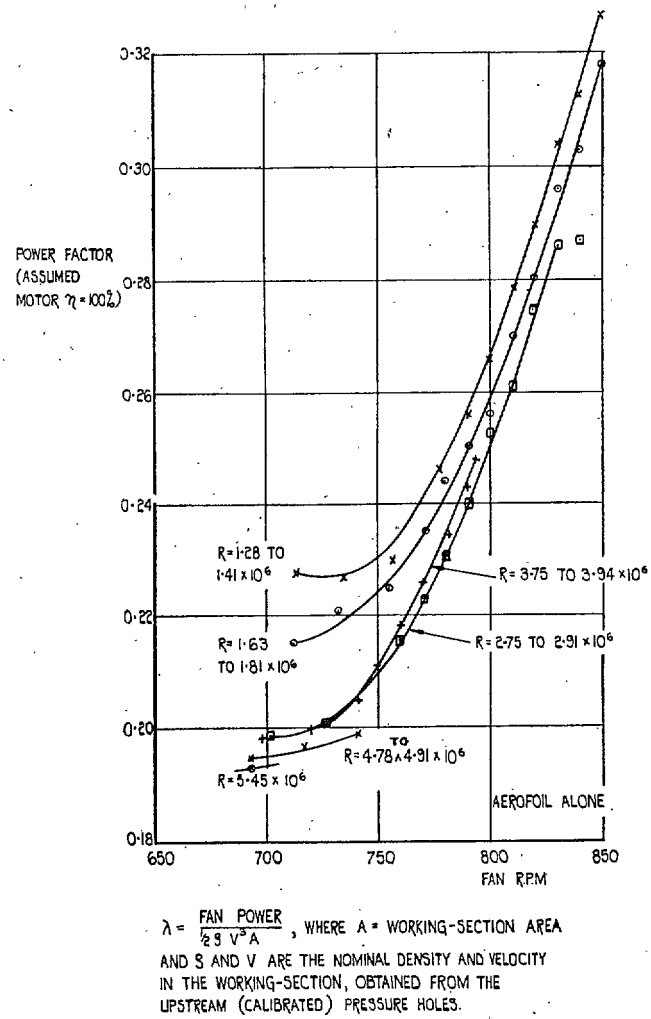

FIG. 6. High-Speed Tunnel power factor at choking with a 37·5-in. chord NACA 0015 aerofoil.

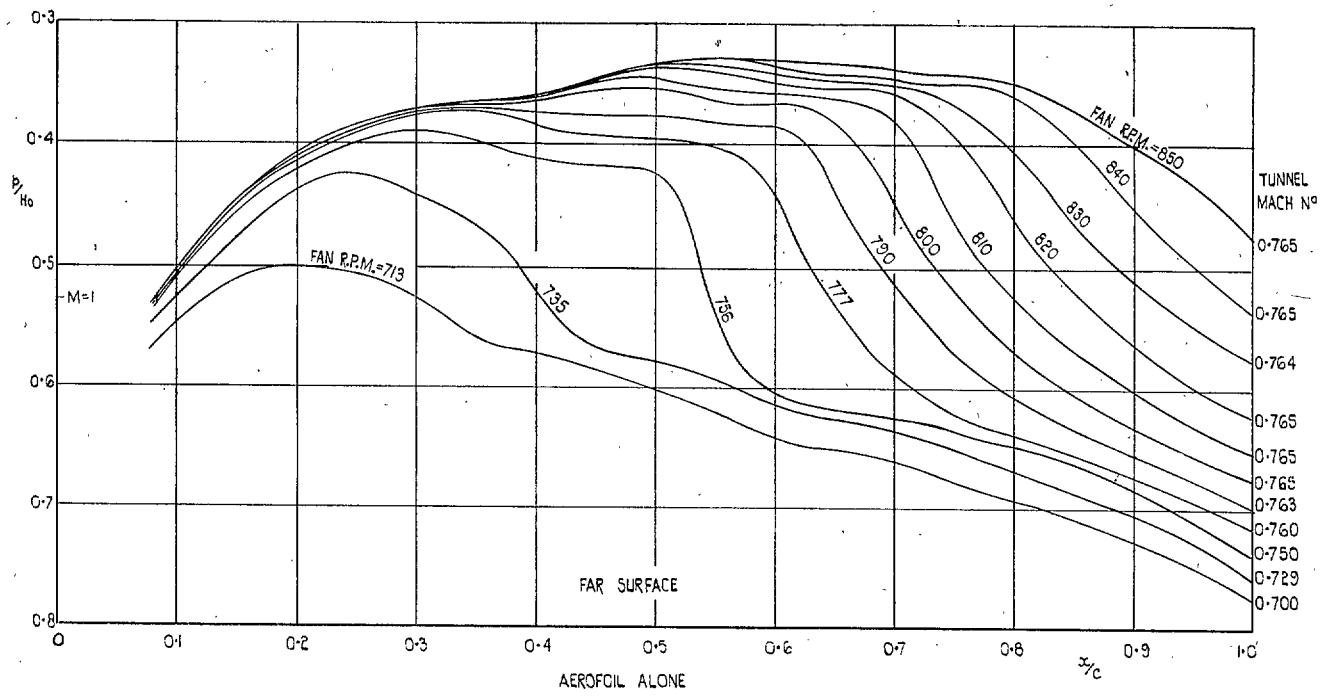

FIG. 7a. Pressure distribution on aerofoil surface during development of choking. $R = 1{\cdot}4 \times 10^6$.

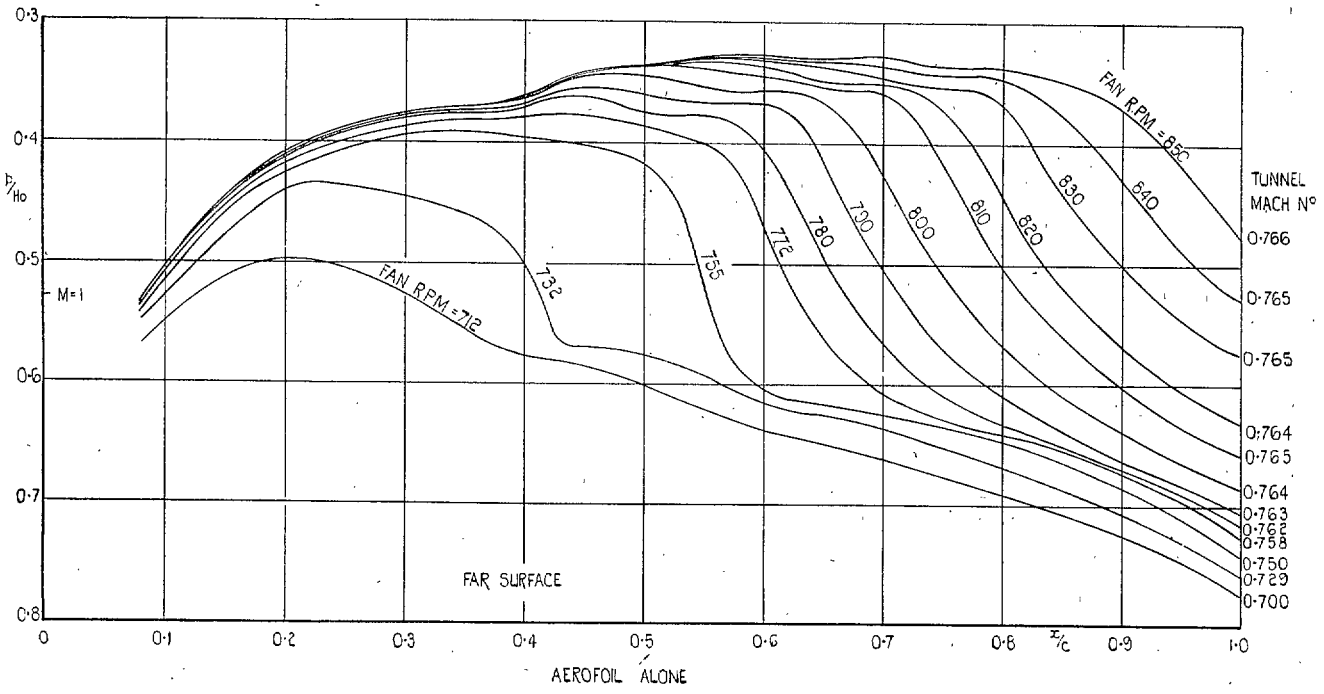

FIG. 7b. Pressure distribution on aerofoil surface during development of choking. $R = 1{\cdot}8 \times 10^6$.

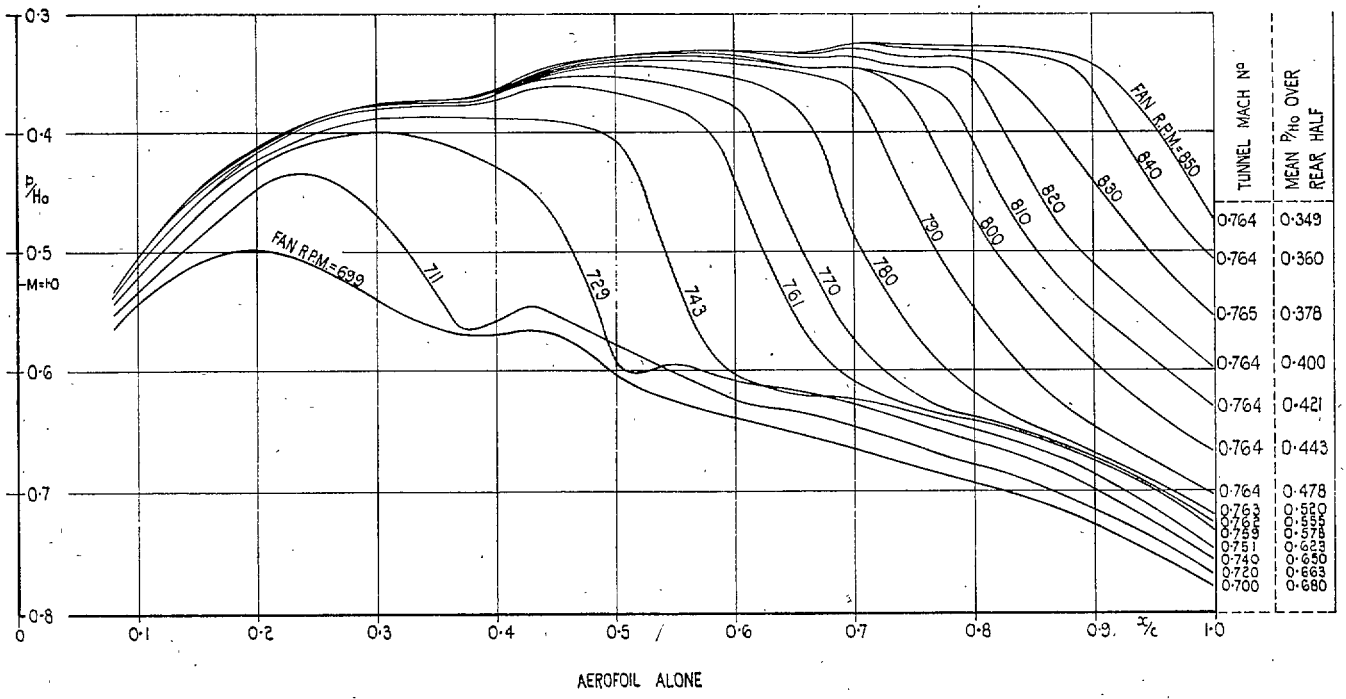

FIG. 7c. Pressure distribution on aerofoil surface during development of choking. $R = 2{\cdot}8 \times 10^6$.

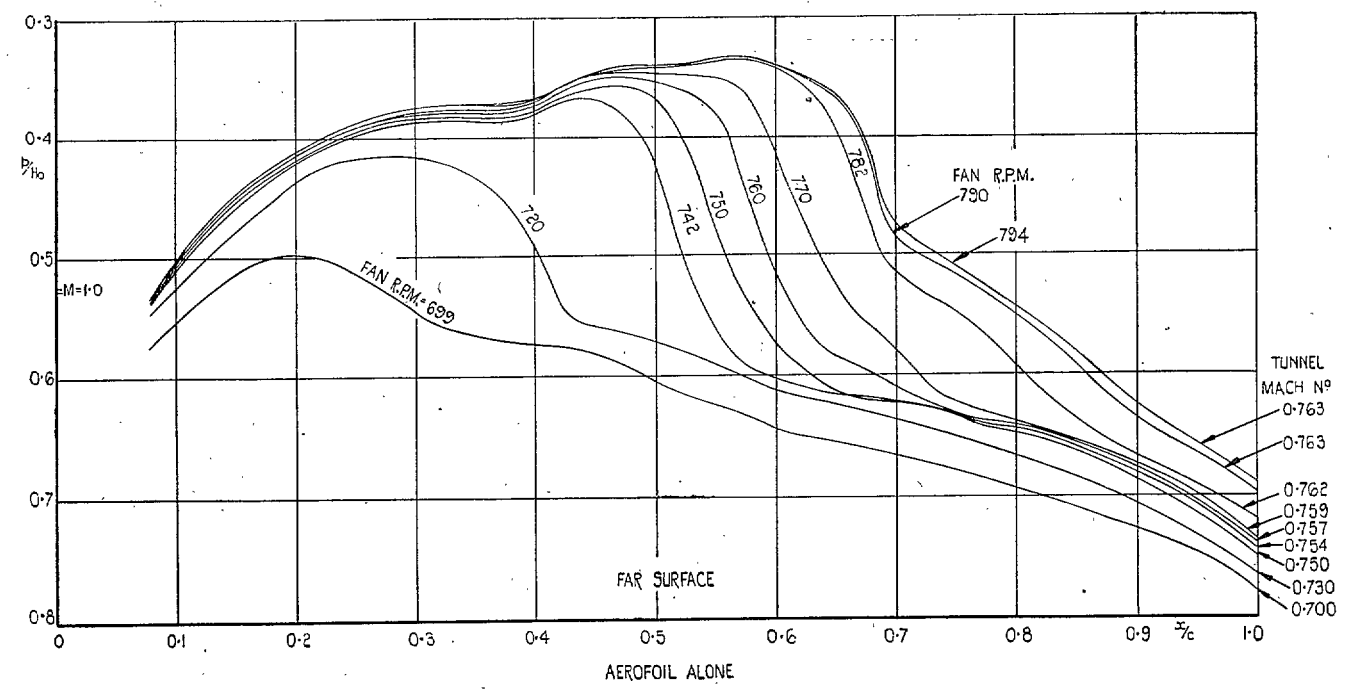

FIG. 7d. Pressure distribution on aerofoil surface during development of choking. $R = 3{\cdot}8 \times 10^6$.

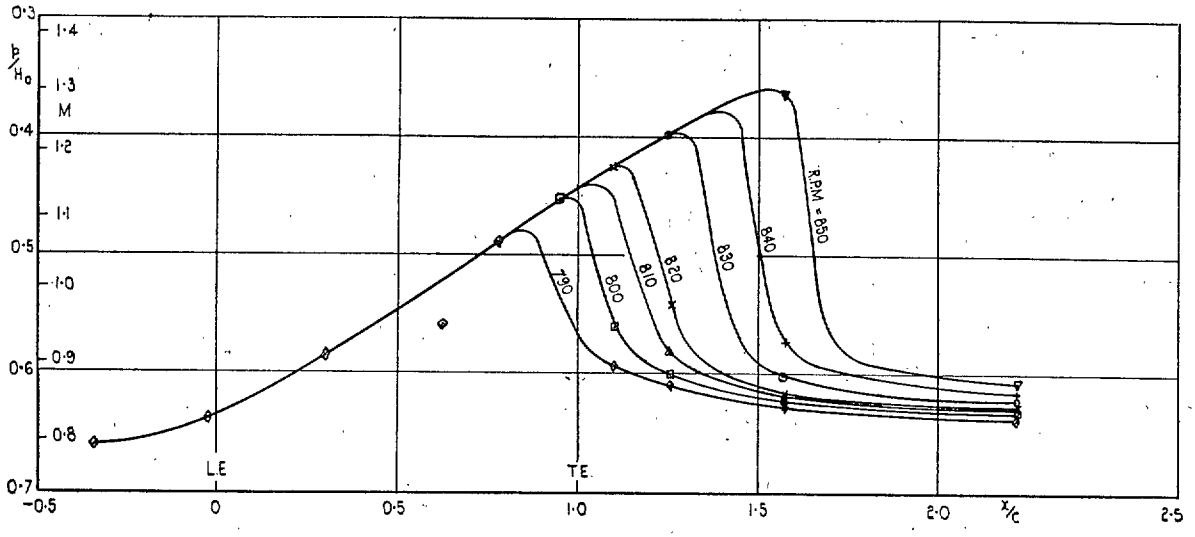

FIG. 8. Pressure distribution on wall (far side) when tunnel is choked. Aerofoil alone. $R = 2{\cdot}8 \times 10^6$.

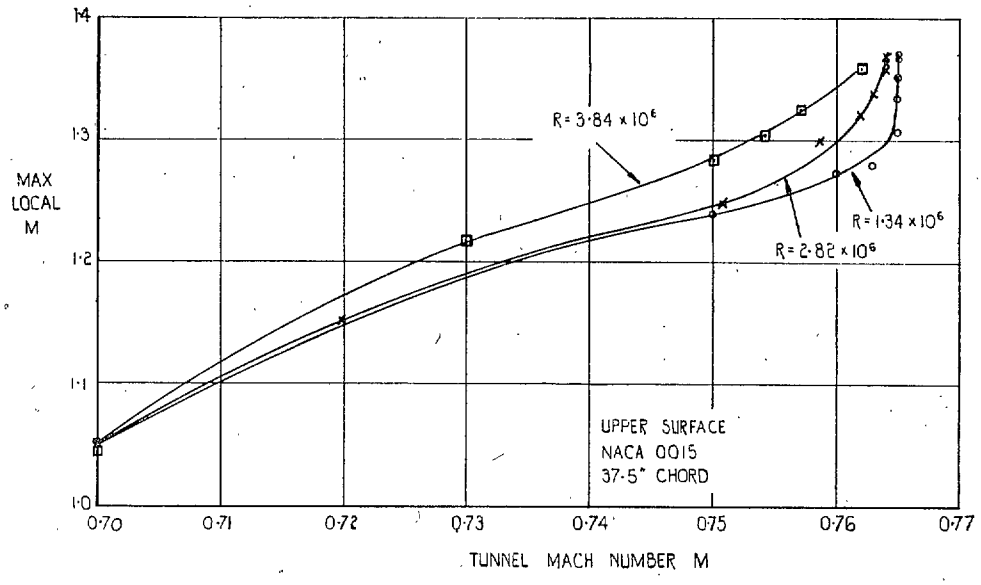

FIG. 9. Maximum Mach number on aerofoil surface.

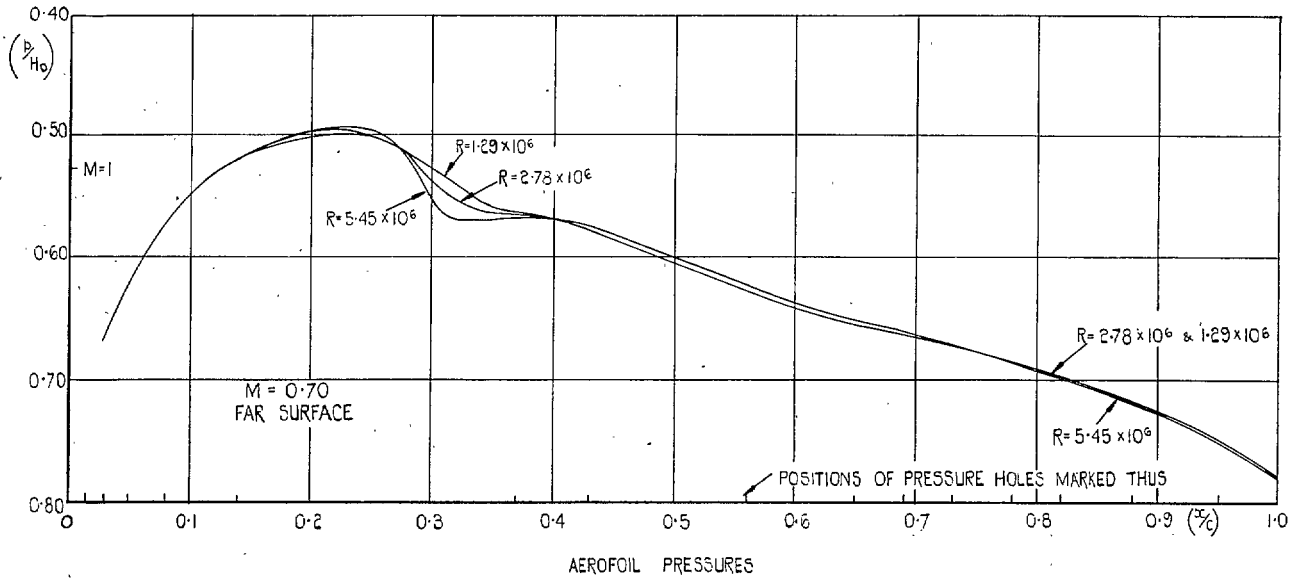

FIG. 10a. Reynolds number effect at constant M.

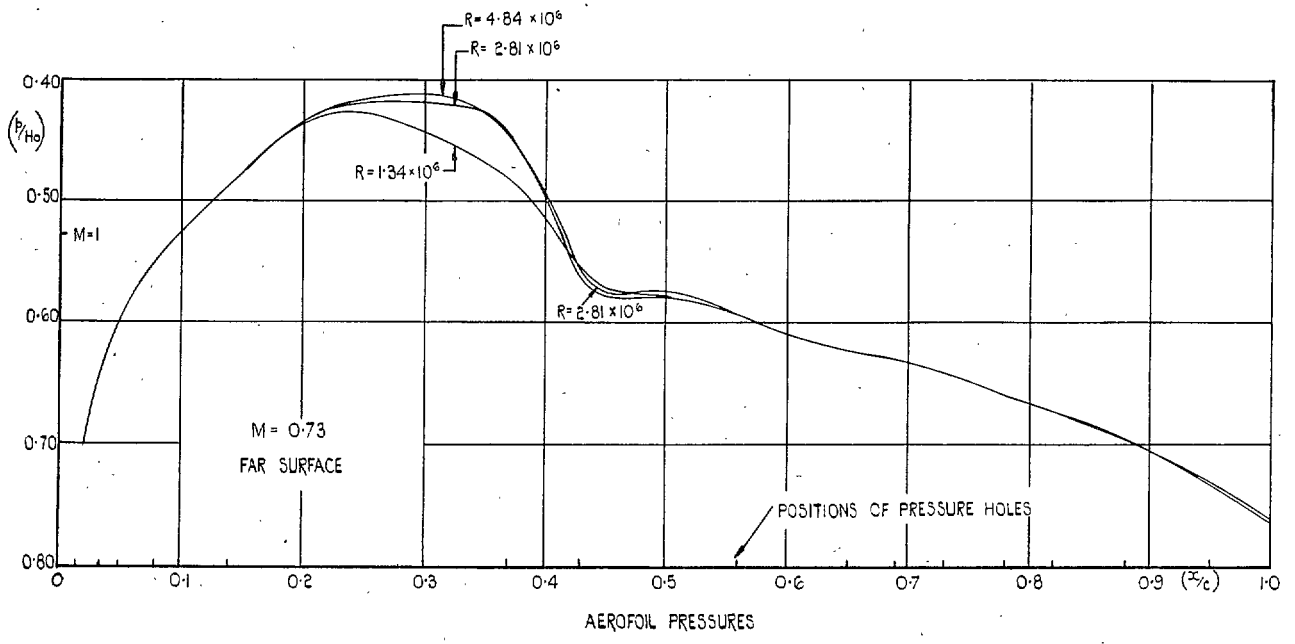

FIG. 10b. Reynolds number effect at constant M.

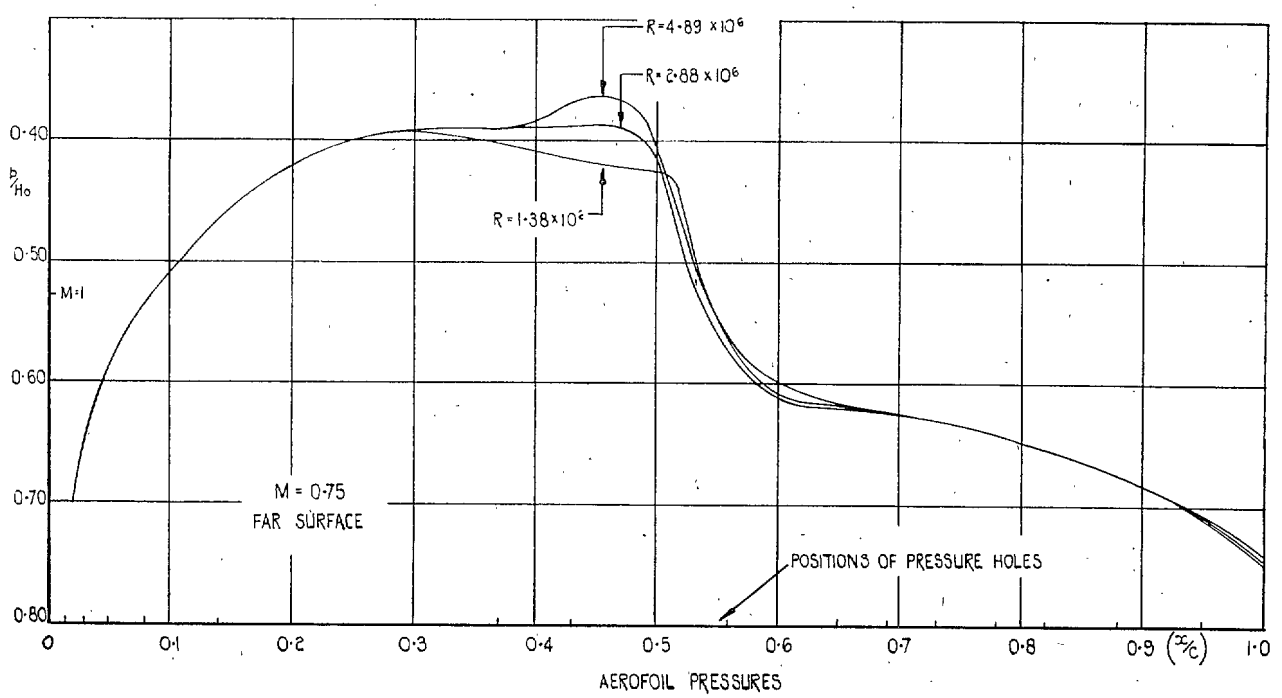

FIG. 10c. Reynolds number effect at constant M.

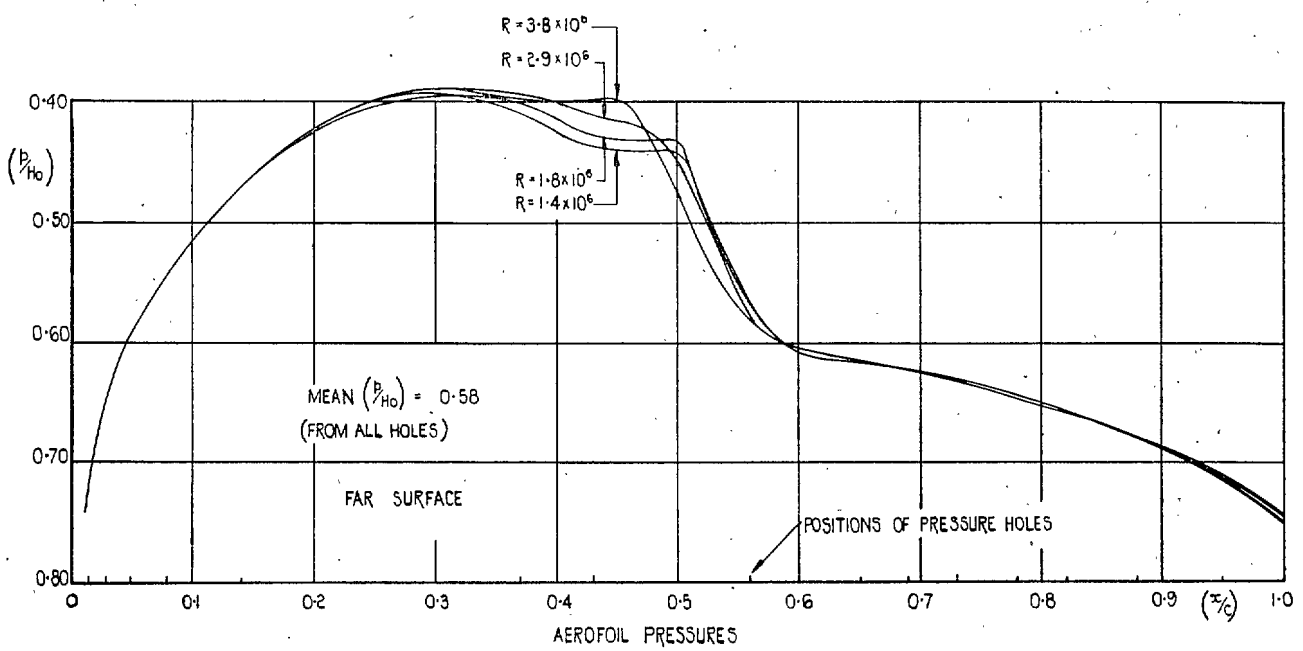

FIG. 11a. Reynolds number effect at constant mean p/H_0.

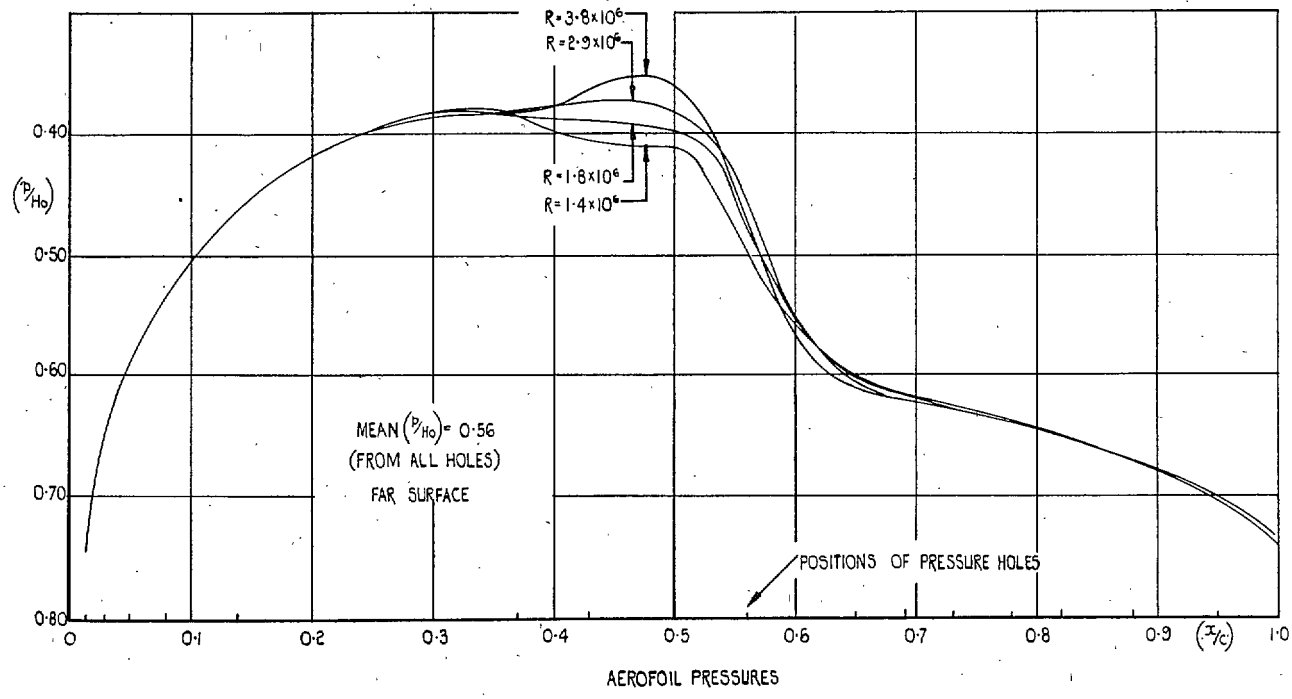

FIG. 11b. Reynolds number effect at constant mean p/H_0.

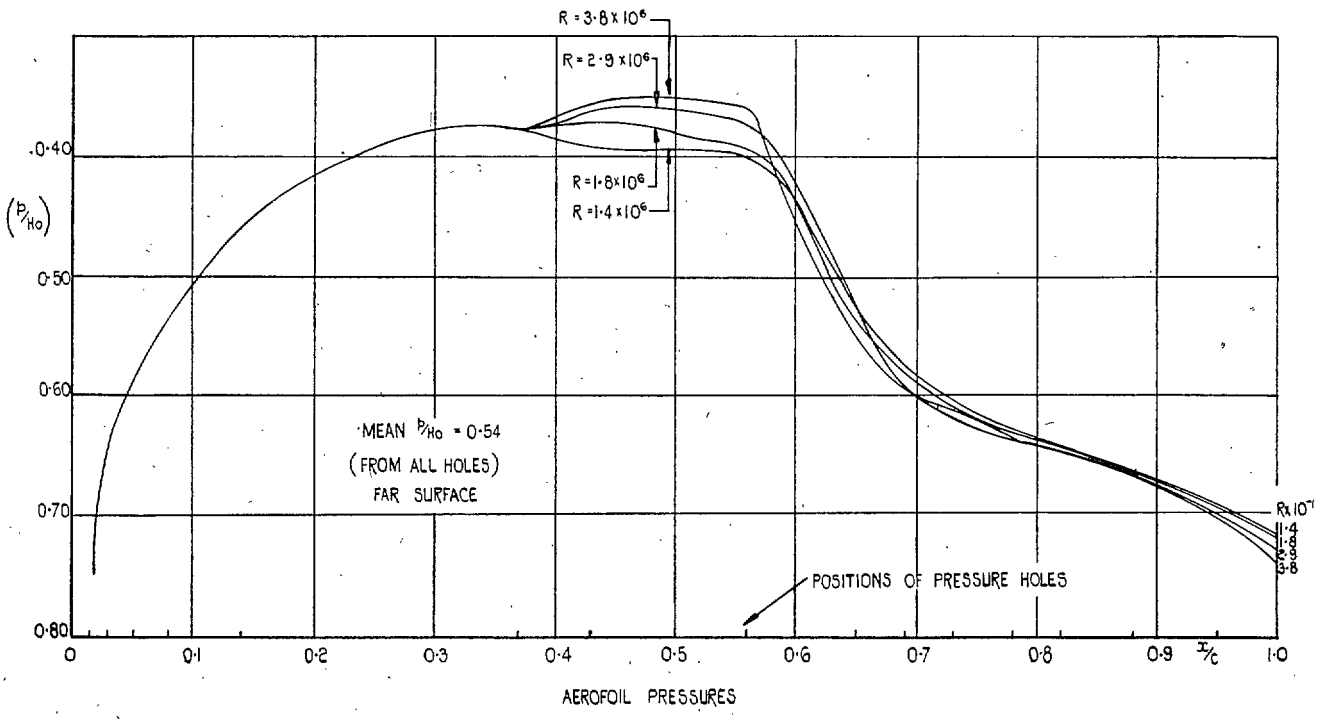

FIG. 11c. Reynolds number effect at constant mean p/H_0.

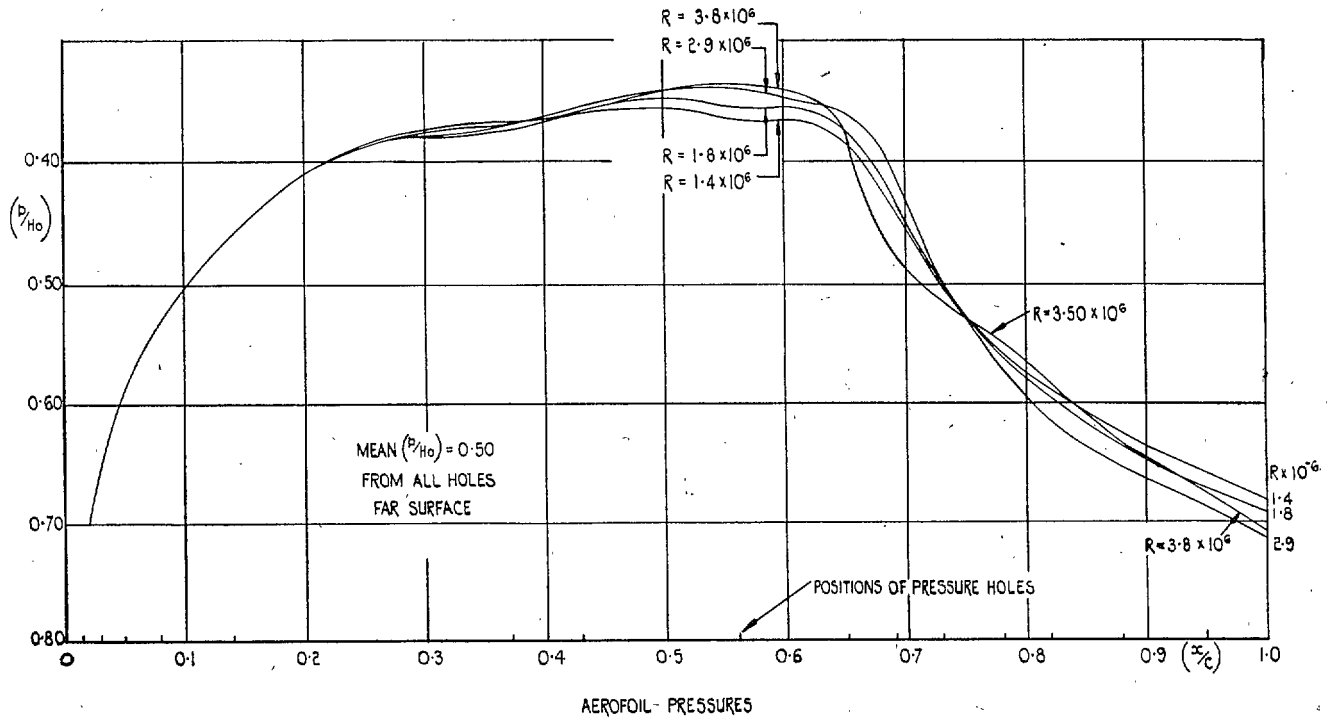

FIG. 11d. Reynolds number effect at constant mean p/H_0.

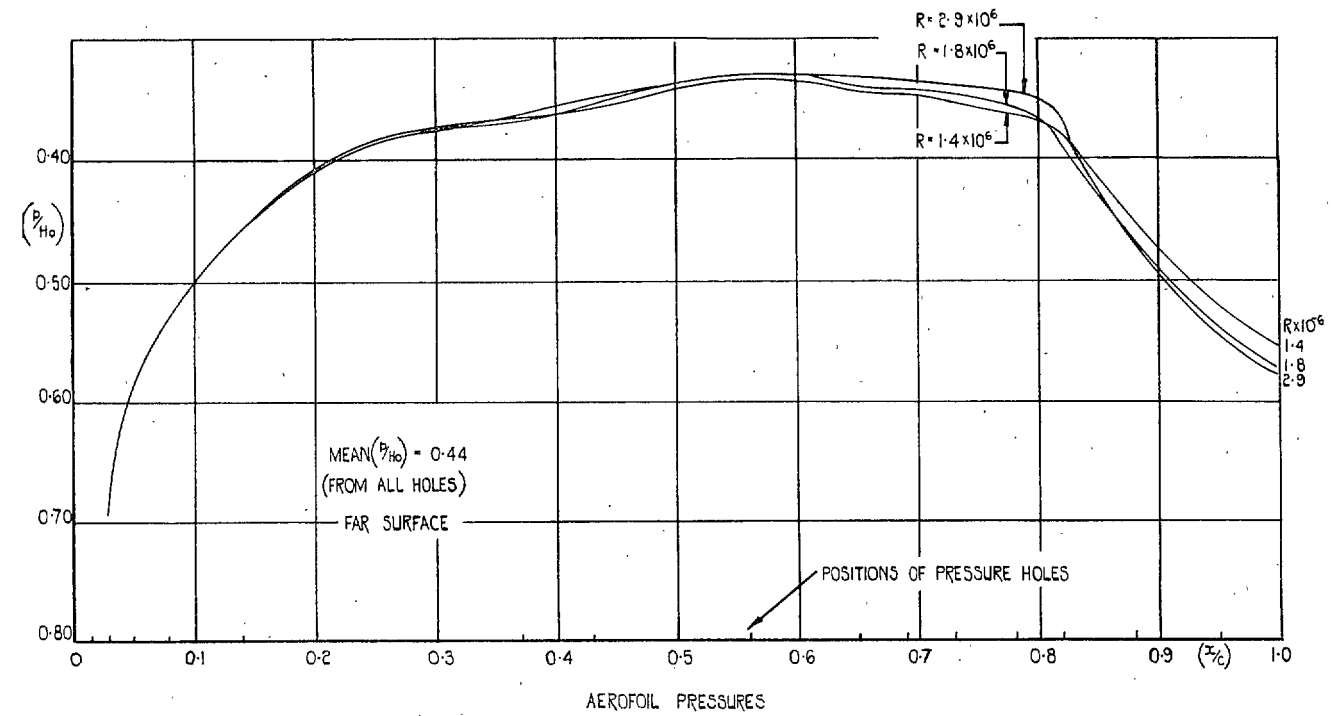

FIG. 11e. Reynolds number effect at constant mean p/H_0.

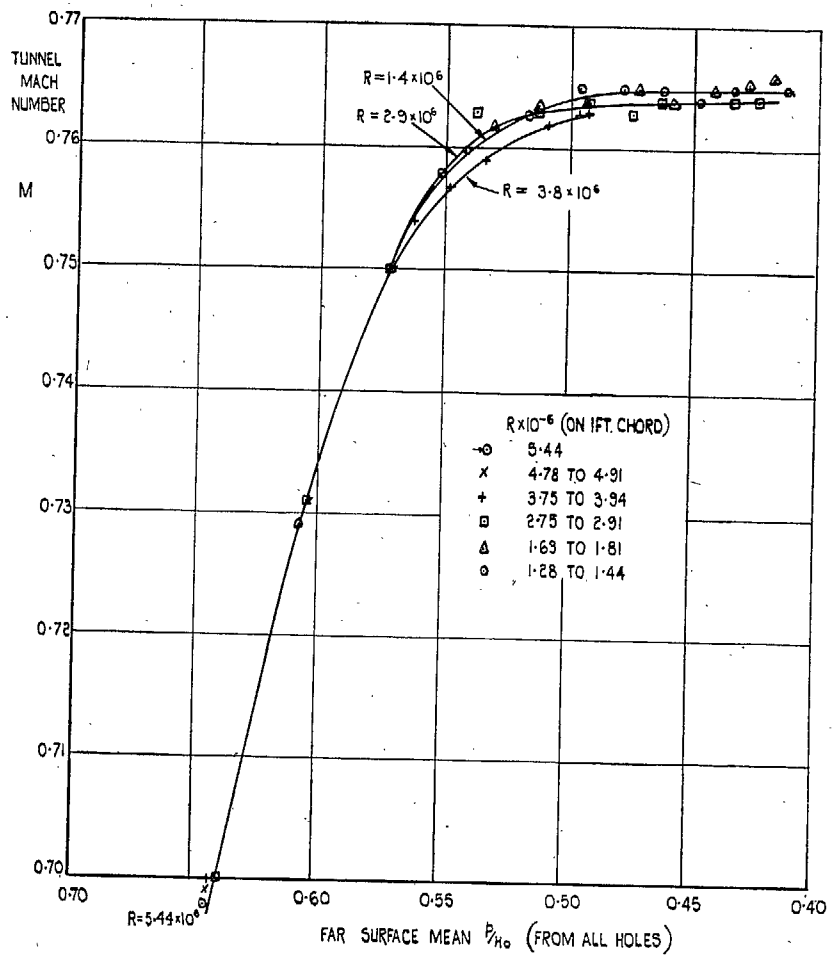

FIG. 12a. Tunnel Mach number *vs.* mean p/H_0.

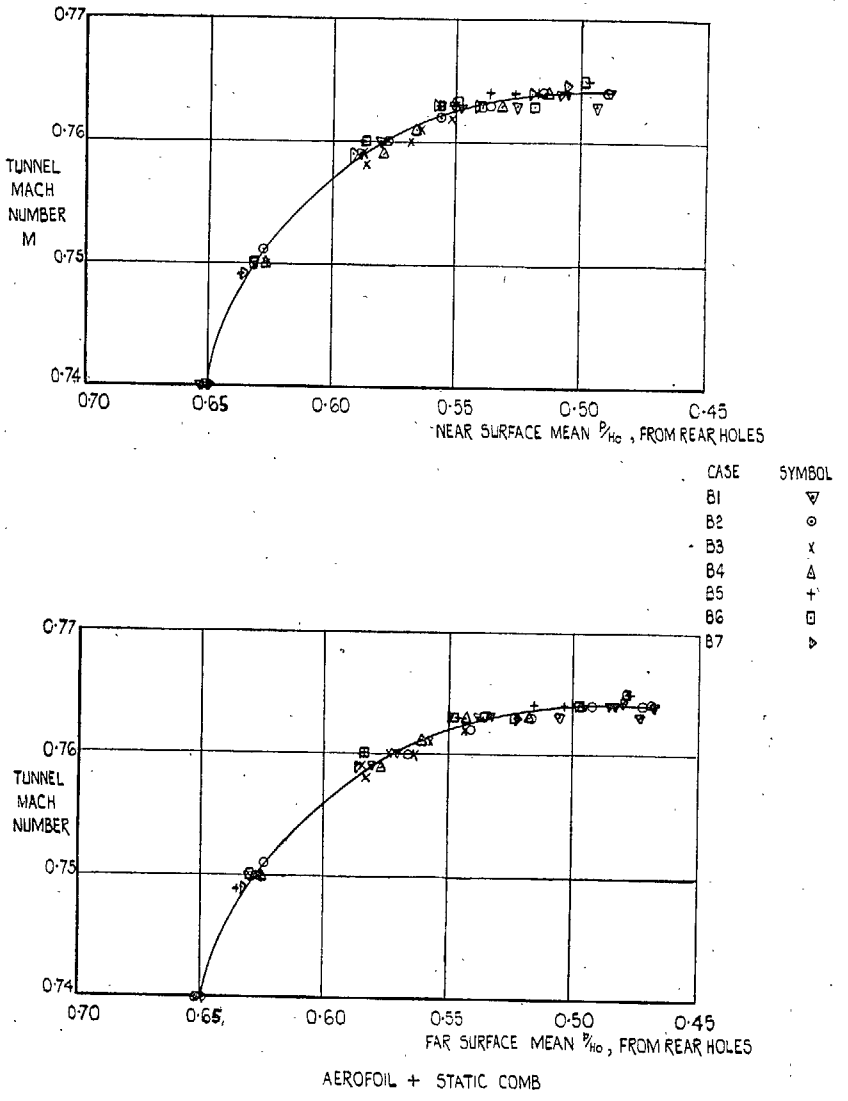

FIG. 12b. Tunnel Mach number *vs.* mean p/H_0. $R = 2{\cdot}8 \times 10^6$.

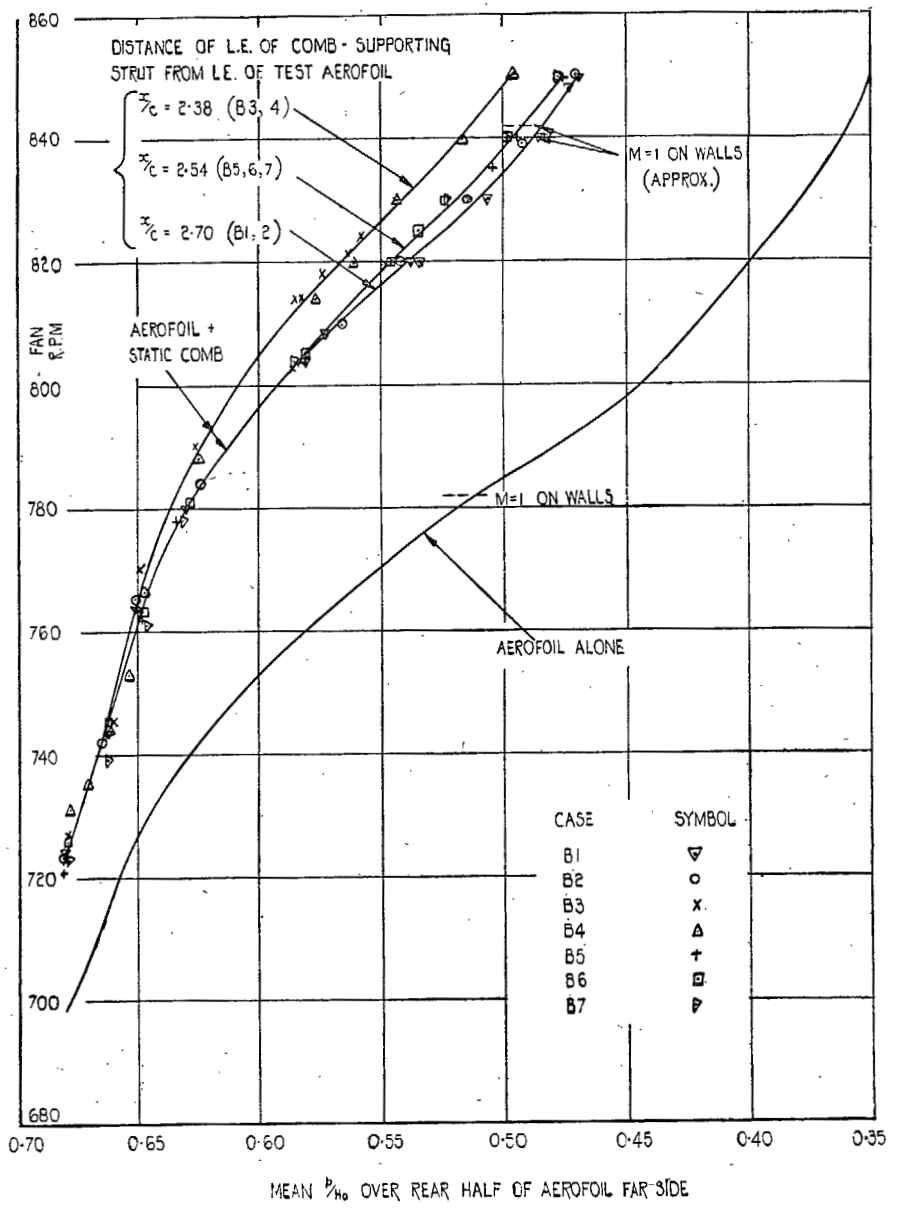

FIG. 14. Relation between fan r.p.m. and mean p/H_0. $R = 2{\cdot}8 \times 10^6$.

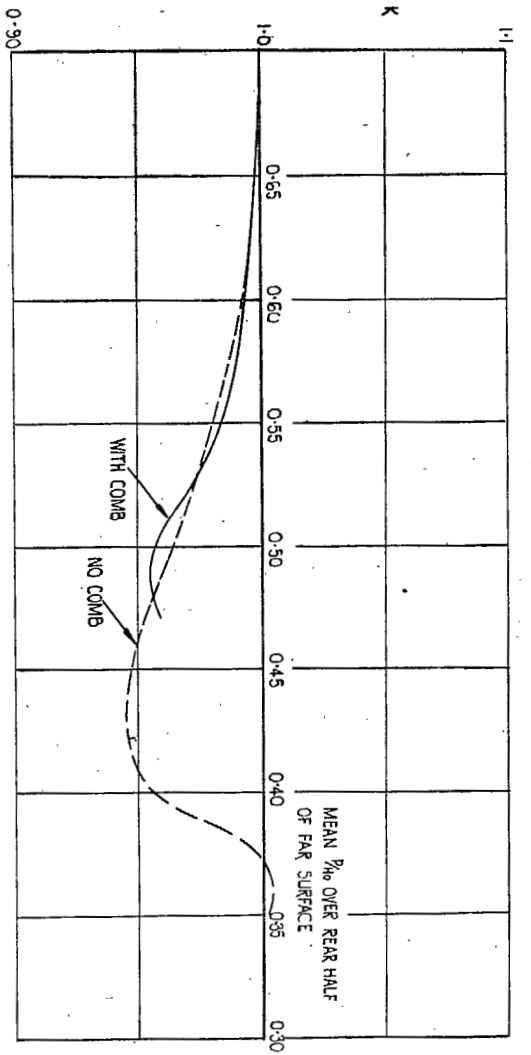

$K = \dfrac{\text{MEAN } p/H \text{ OVER REAR HALF OF FAR SURFACE}}{\text{MEAN } p/H \text{ OVER REAR HALF OF NEAR SURFACE}}$

$R = 2{\cdot}8 \times 10^6$

FIG. 13. Asymmetry of flow at choking.

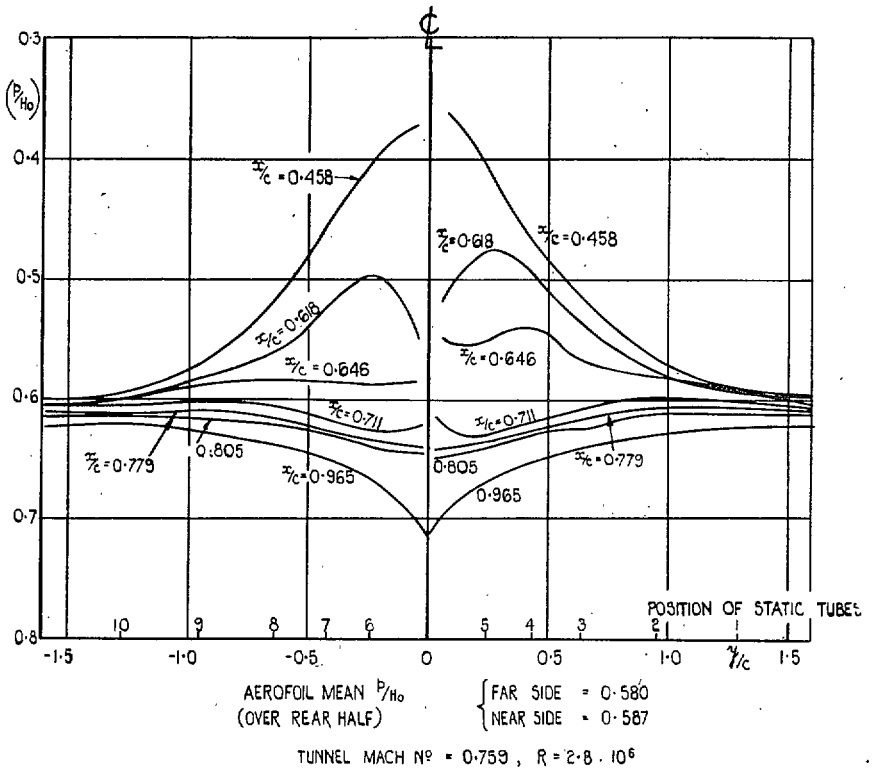

FIG. 15a. Static pressures across tunnel.

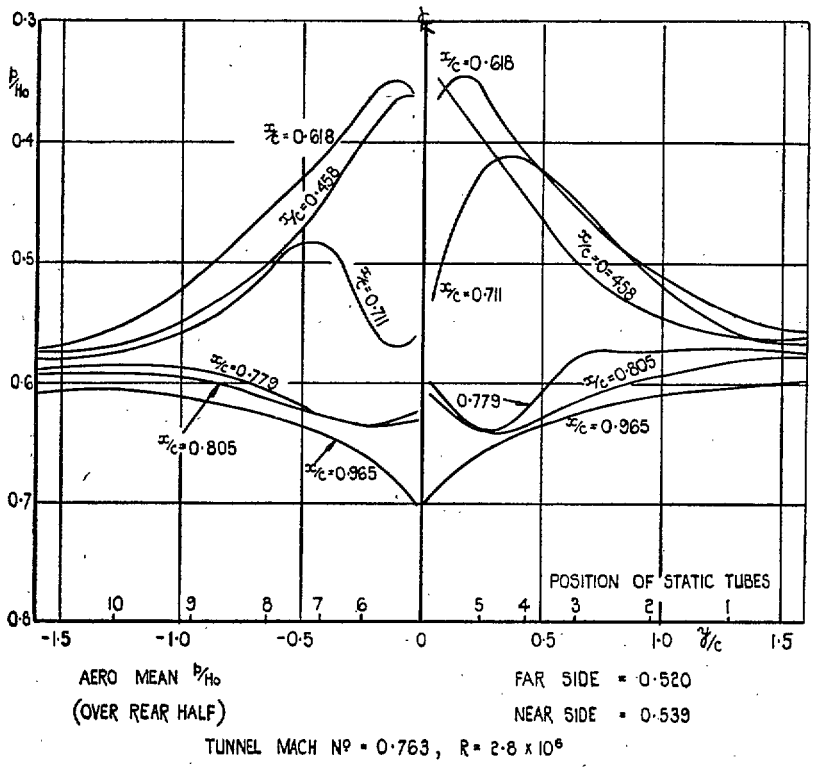

FIG. 15b. Static pressures across tunnel.

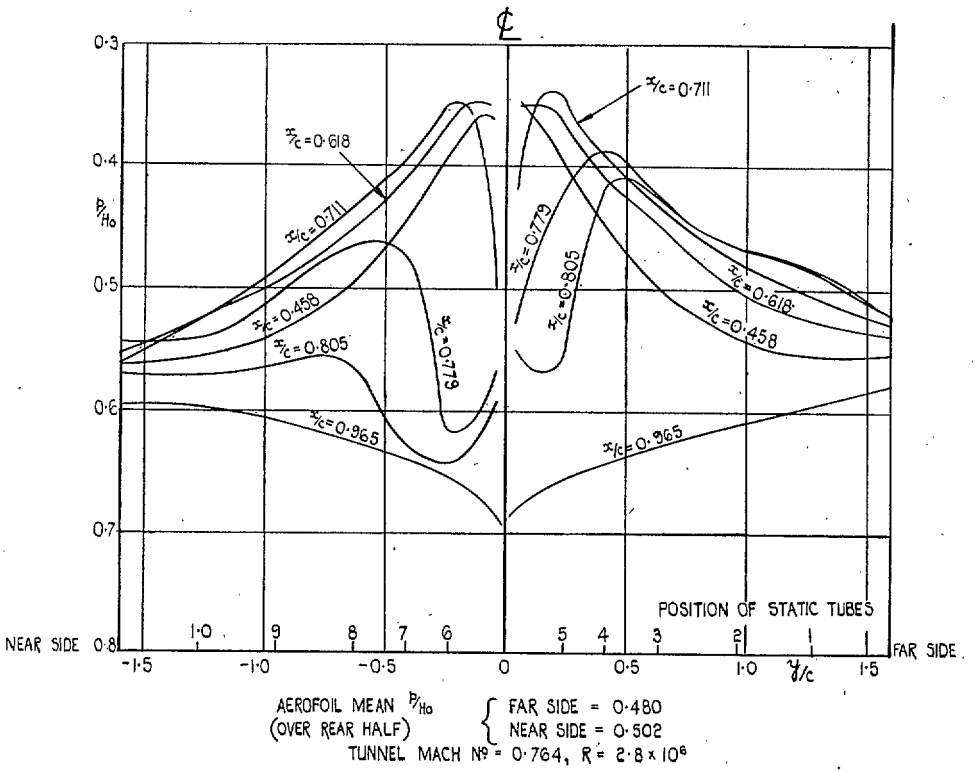

FIG. 15c. Static pressures across tunnel.

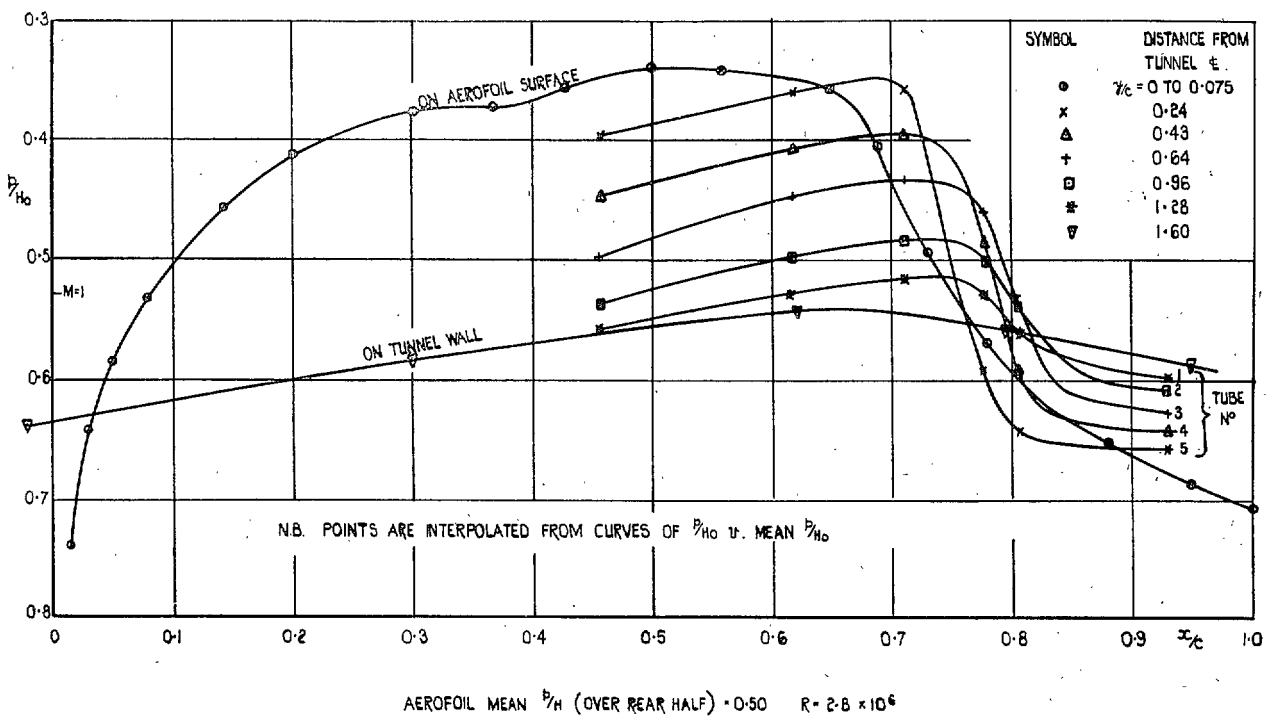

FIG. 16. Example of static pressures along tunnel on far side.

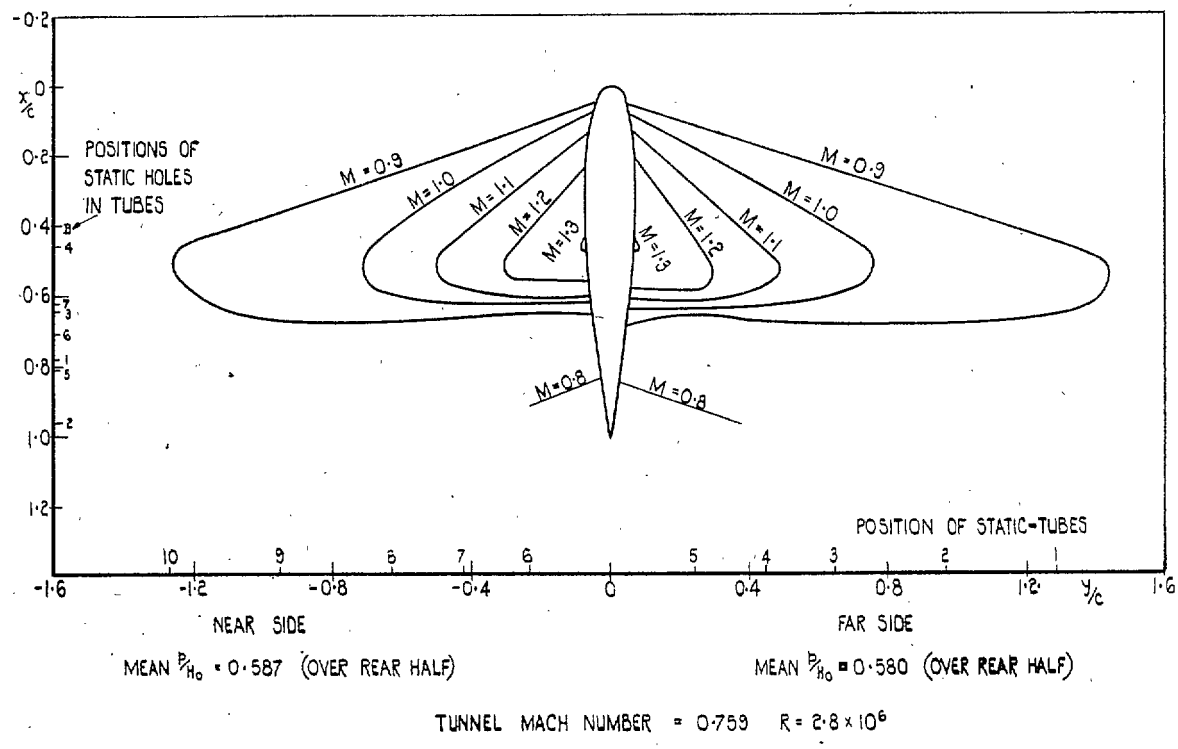

FIG. 17a. Mach number distribution.

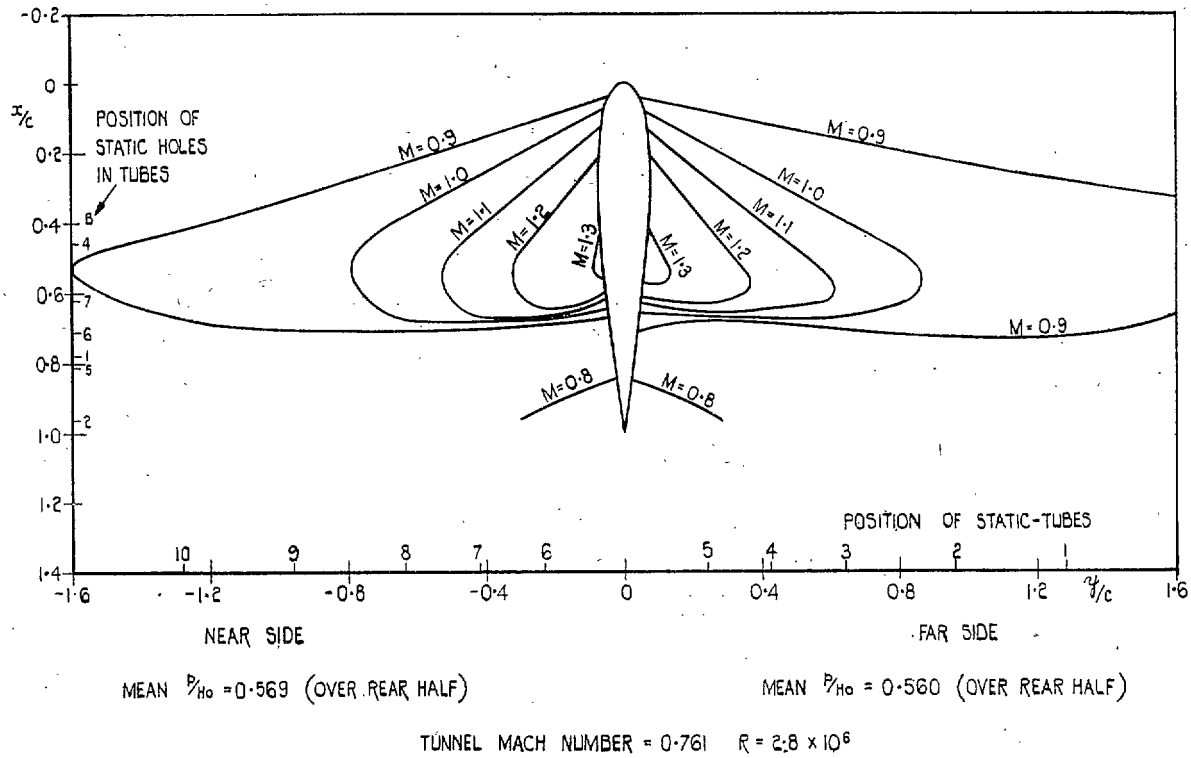

FIG. 17b. Mach number distribution.

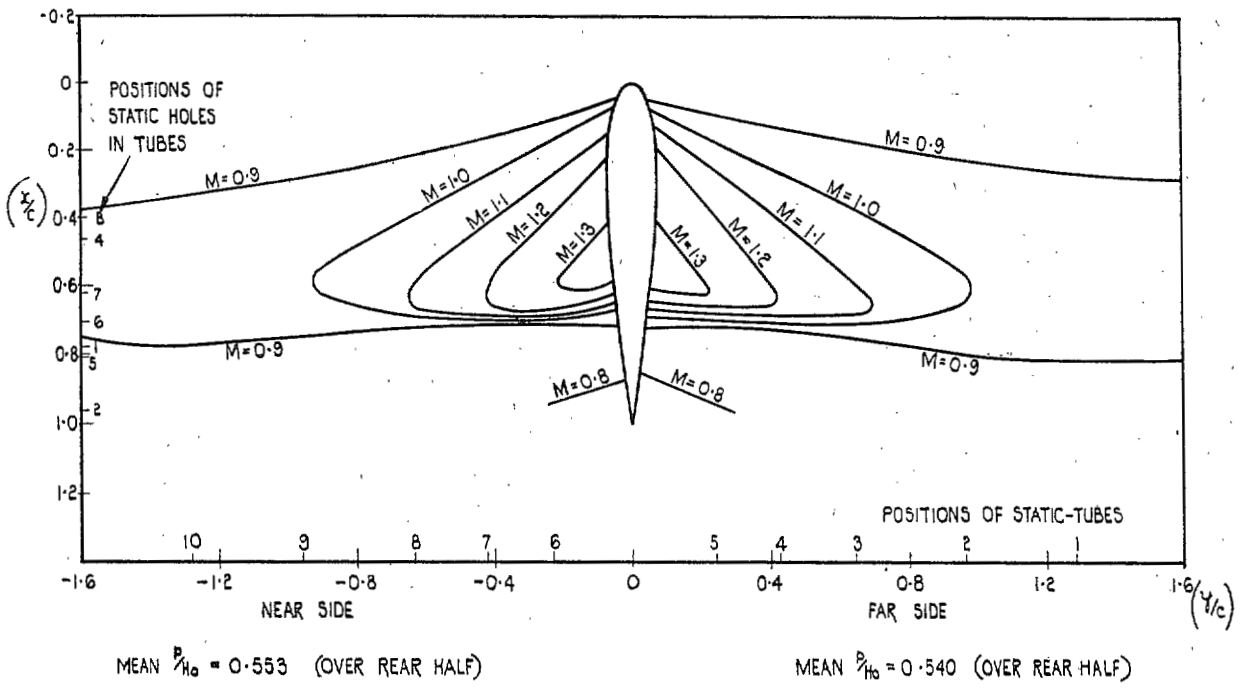

MEAN p/H_0 = 0·553 (OVER REAR HALF) MEAN p/H_0 = 0·540 (OVER REAR HALF)

TUNNEL MACH NUMBER = 0·762 , R = 2·8 × 10^6

FIG. 17c. Mach number distribution.

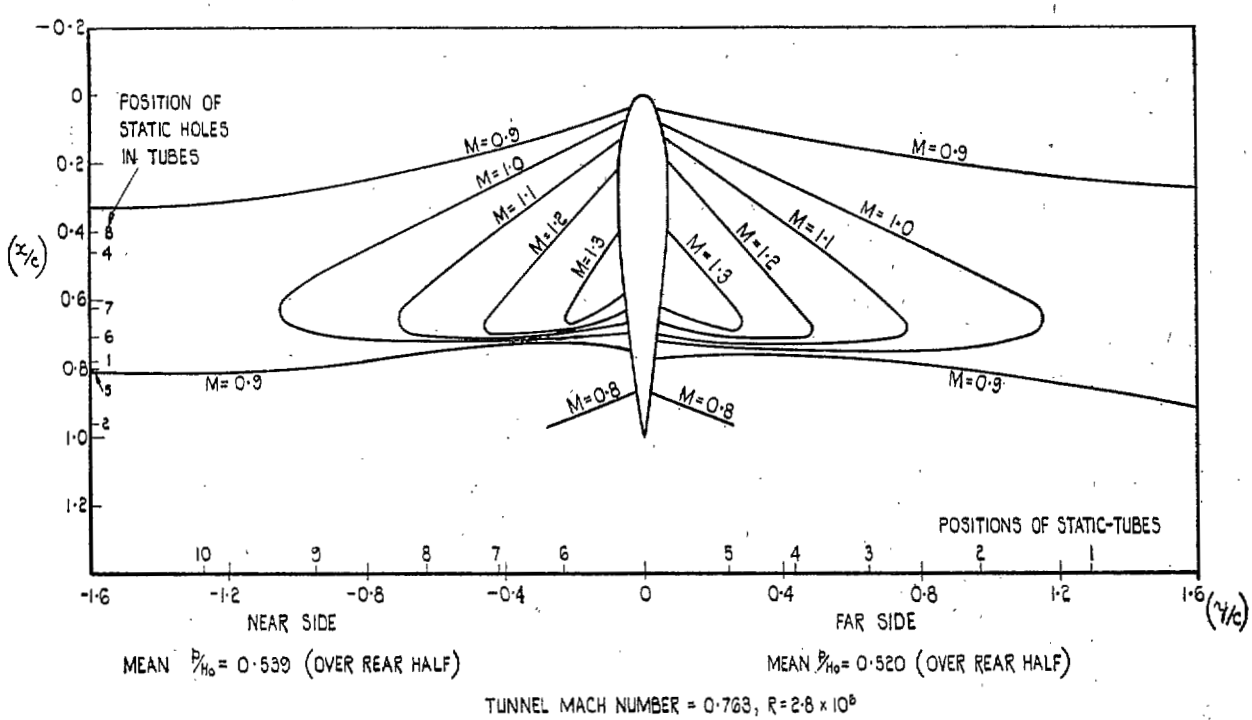

MEAN p/H_0 = 0·539 (OVER REAR HALF) MEAN p/H_0 = 0·520 (OVER REAR HALF)

TUNNEL MACH NUMBER = 0·763, R = 2·8 × 10^6

FIG. 17d. Mach number distribution.

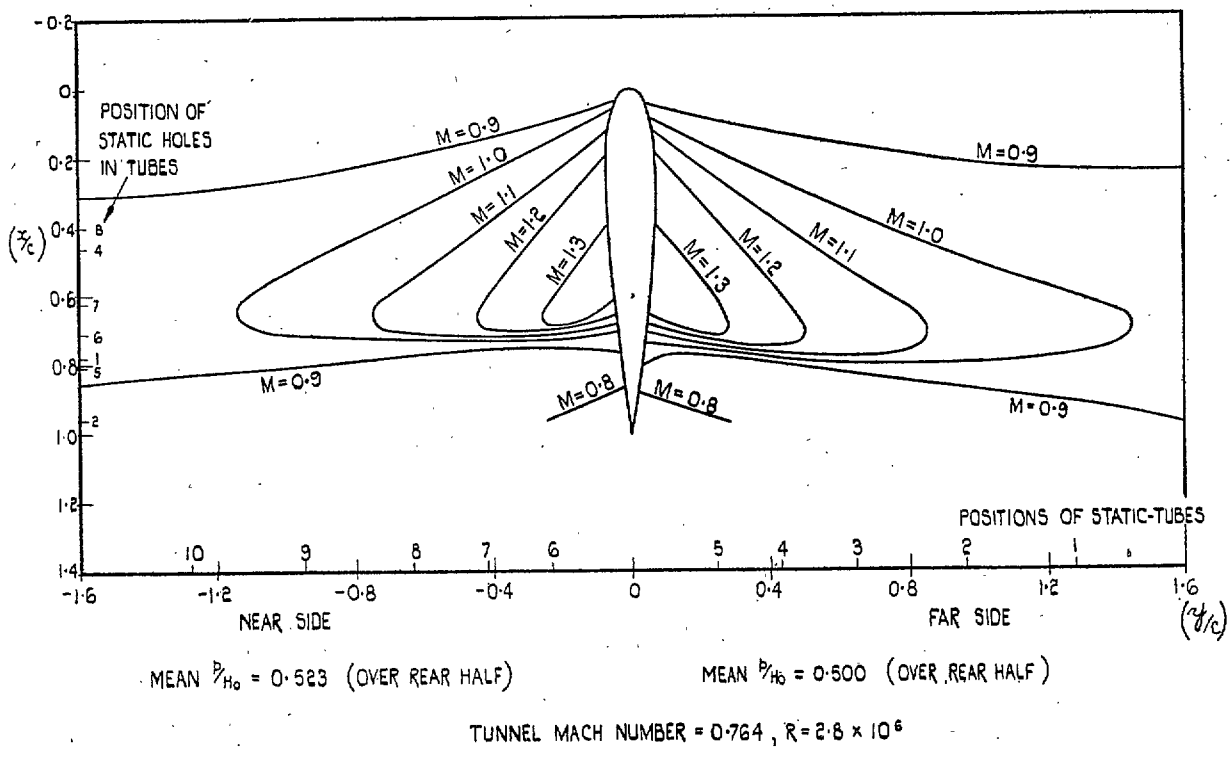

FIG. 17e. Mach number distribution.

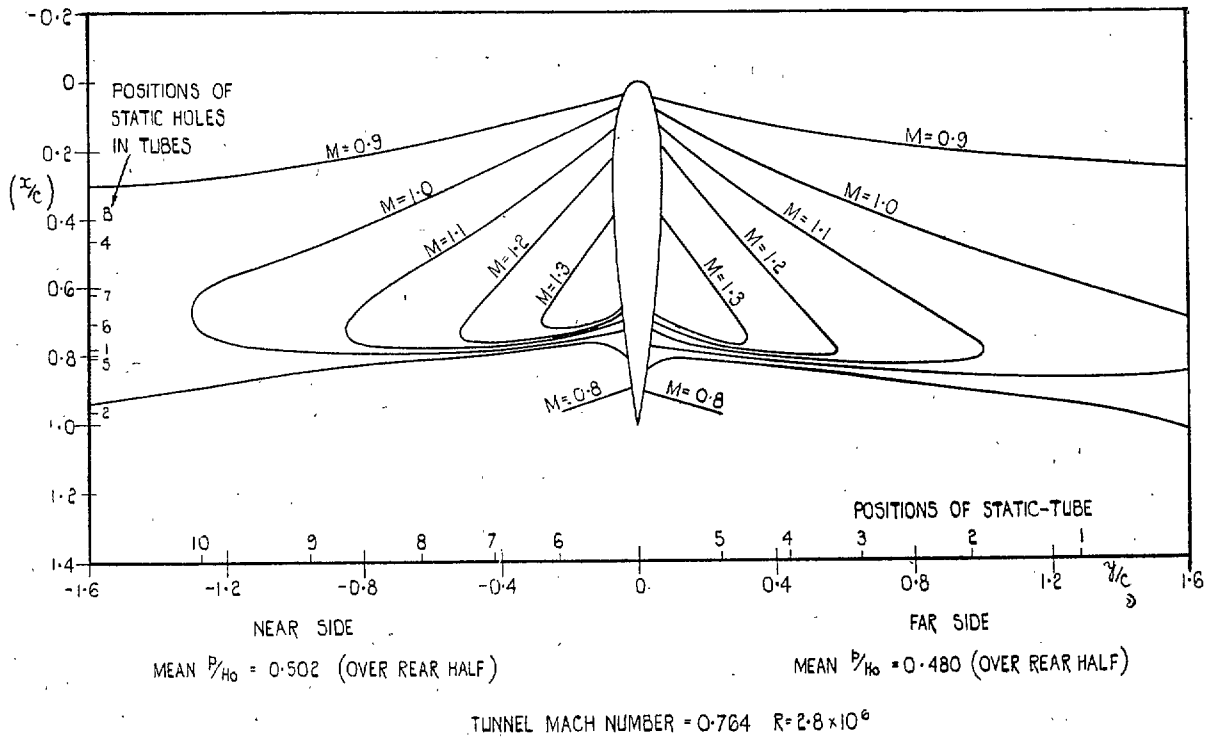

FIG. 17f. Mach number distribution.

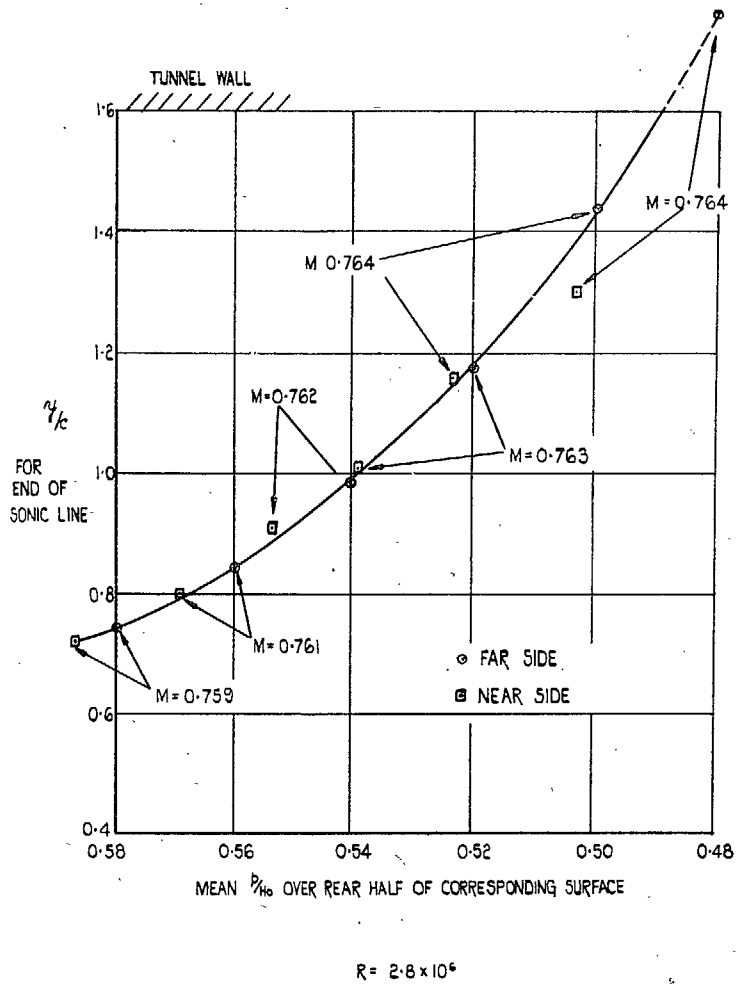

FIG. 19a. Extent of supersonic region. y/c vs. mean p/H_0.

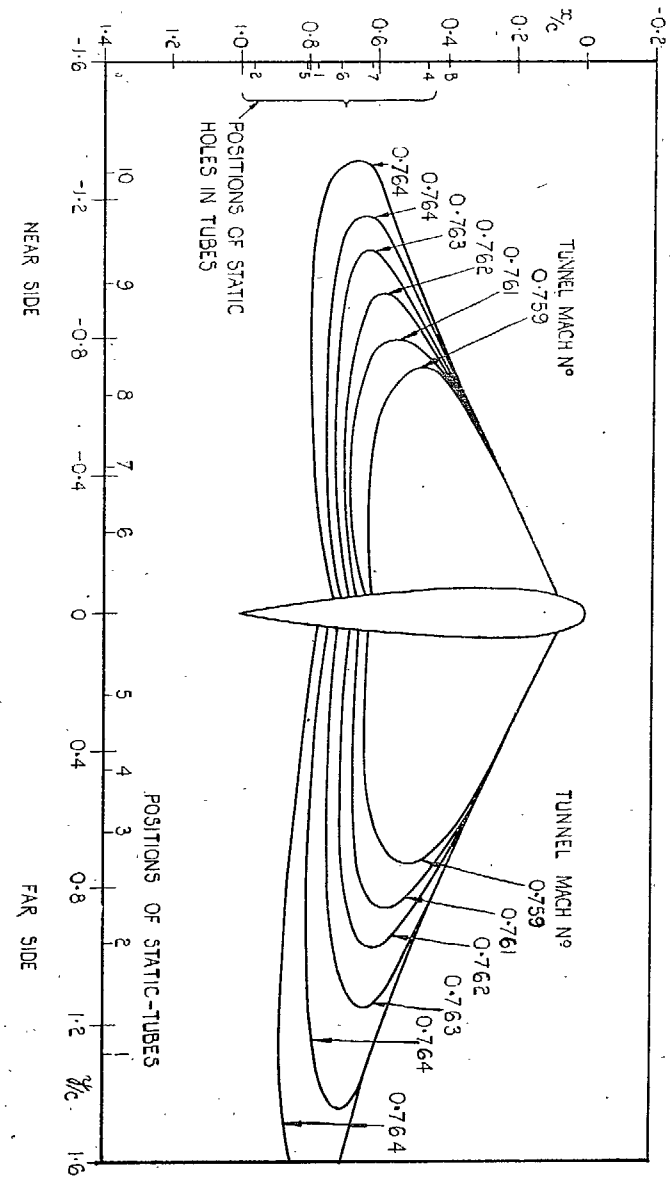

FIG. 18. Position of sonic line.

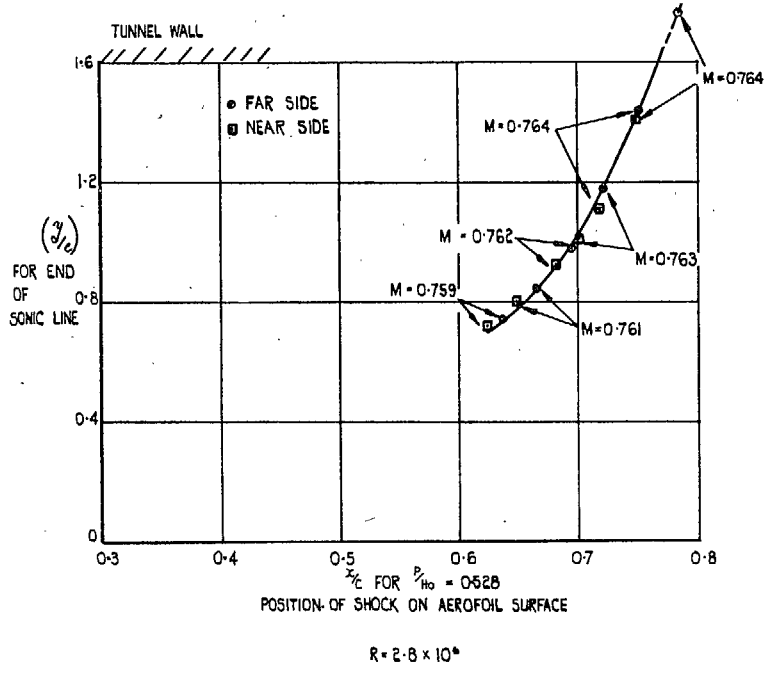

FIG. 19b. Extent of supersonic region. y/c vs. x/c aerofoil.

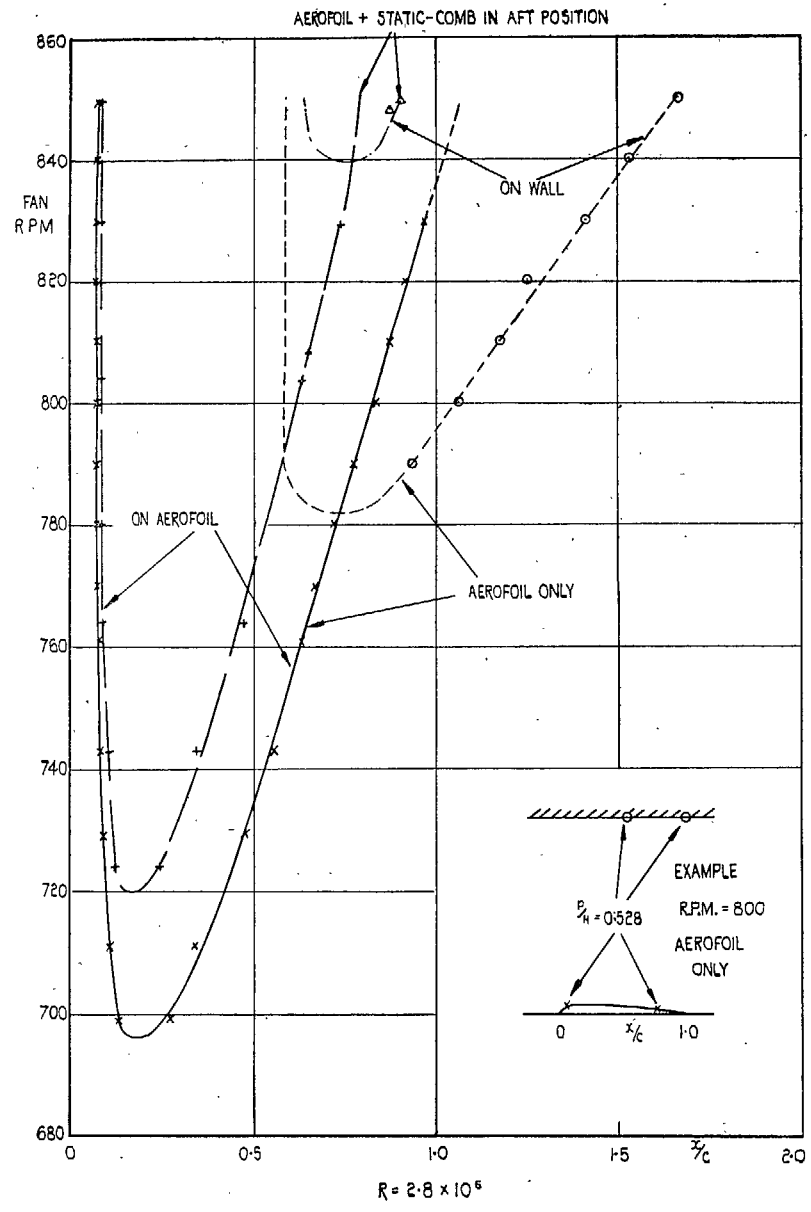

FIG. 20. Fore-and-aft location of points on aerofoil and walls where $p/H = 0 \cdot 528$ ($M = 1$).

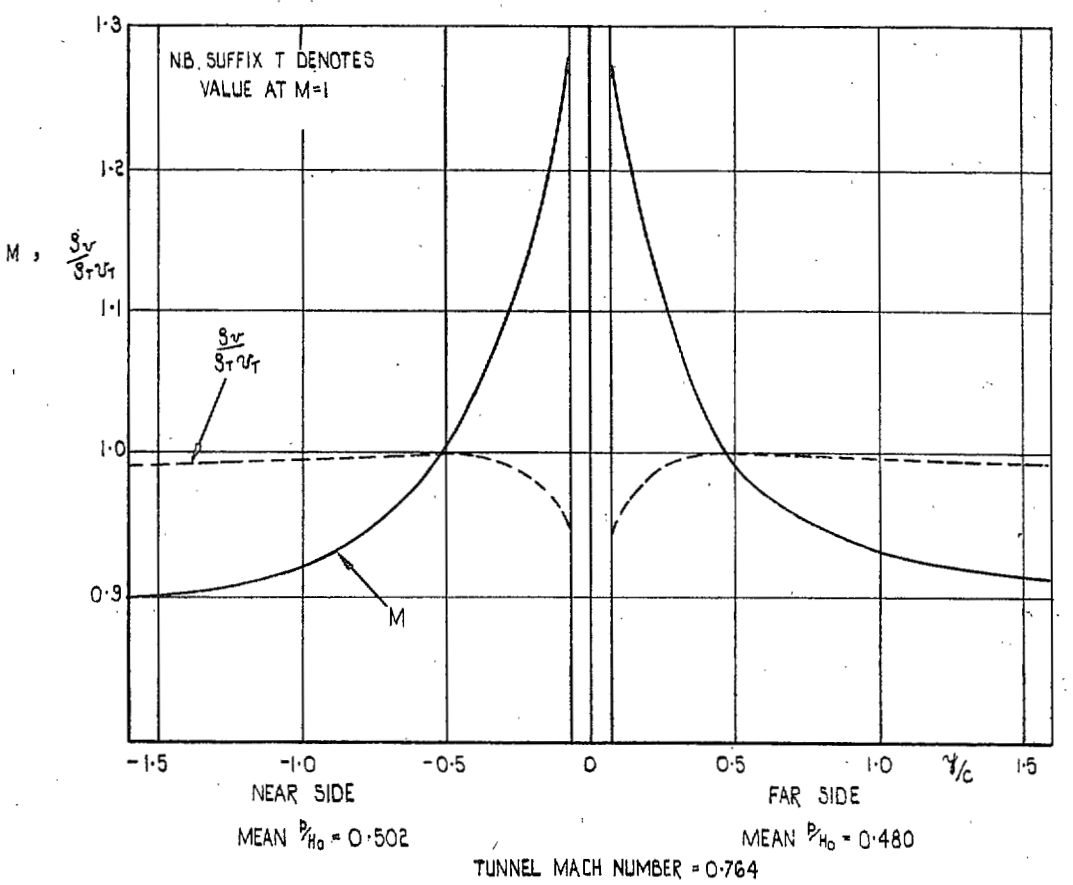

FIG. 21. Typical Mach number and mass flow distributions across tunnel at $x/c = 0{\cdot}30$.

Wt. 17/680 K.7 7/55 G.G. 34–262

PRINTED IN GREAT BRITAIN

Publications of the Aeronautical Research Council

ANNUAL TECHNICAL REPORTS OF THE AERONAUTICAL RESEARCH COUNCIL (BOUND VOLUMES)

1936 Vol. I. Aerodynamics General, Performance, Airscrews, Flutter and Spinning. 40*s*. (41*s*. 1*d*.)
Vol. II. Stability and Control, Structures, Seaplanes, Engines, etc. 50*s*. (51*s*. 1*d*.)

1937 Vol. I. Aerodynamics General, Performance, Airscrews, Flutter and Spinning. 40*s*. (41*s*. 1*d*.)
Vol. II. Stability and Control, Structures, Seaplanes, Engines, etc. 60*s*. (61*s*. 1*d*.)

1938 Vol. I. Aerodynamics General, Performance, Airscrews. 50*s*. (51*s*. 1*d*.)
Vol. II. Stability and Control, Flutter, Structures, Seaplanes, Wind Tunnels, Materials. 30*s*. (31*s*. 1*d*.)

1939 Vol. I. Aerodynamics General, Performance, Airscrews, Engines. 50*s*. (51*s*. 1*d*.)
Vol. II. Stability and Control, Flutter and Vibration, Instruments, Structures, Seaplanes, etc. 63*s*. (64*s*. 2*d*.)

1940 Aero and Hydrodynamics, Aerofoils, Airscrews, Engines, Flutter, Icing, Stability and Control, Structures, and a miscellaneous section. 50*s*. (51*s*. 1*d*.)

1941 Aero and Hydrodynamics, Aerofoils, Airscrews, Engines, Flutter, Stability and Control, Structures. 63*s*. (64*s*. 2*d*.)

1942 Vol. I. Aero and Hydrodynamics, Aerofoils, Airscrews, Engines. 75*s*. (76*s*. 3*d*.)
Vol. II. Noise, Parachutes, Stability and Control, Structures, Vibration, Wind Tunnels. 47*s*. 6*d*. (48*s*. 7*d*.)

1943 Vol. I. Aerodynamics, Aerofoils, Airscrews. 80*s*. (81*s*. 4*d*.)
Vol. II. Engines, Flutter, Materials, Parachutes, Performance, Stability and Control, Structures. 90*s*. (91*s*. 6*d*.)

1944 Vol. I. Aero and Hydrodynamics, Aerofoils, Aircraft, Airscrews, Controls. 84*s*. (85*s*. 8*d*.)
Vol. II. Flutter and Vibration, Materials, Miscellaneous, Navigation, Parachutes, Performance, Plates and Panels, Stability, Structures, Test Equipment, Wind Tunnels. 84*s*. (85*s*. 8*d*.)

Annual Reports of the Aeronautical Research Council—

1933–34	1*s*. 6*d*. (1*s*. 8*d*.)	1937	2*s*. (2*s*. 2*d*.)
1934–35	1*s*. 6*d*. (1*s*. 8*d*.)	1938	1*s*. 6*d*. (1*s*. 8*d*.)
April 1, 1935 to Dec. 31, 1936	4*s*. (4*s*. 4*d*.)	1939–48	3*s*. (3*s*. 2*d*.)

Index to all Reports and Memoranda published in the Annual Technical Reports, and separately—

April, 1950 R. & M. No. 2600. 2*s*. 6*d*. (2*s*. 7½*d*.)

Author Index to all Reports and Memoranda of the Aeronautical Research Council—

1909–1954. R. & M. No. 2570. 15*s*. (15*s*. 4*d*.)

Indexes to the Technical Reports of the Aeronautical Research Council—

December 1, 1936 — June 30, 1939.	R. & M. No. 1850.	1*s*. 3*d*. (1*s*. 4½*d*.)
July 1, 1939 — June 30, 1945.	R. & M. No. 1950.	1*s*. (1*s*. 1½*d*.)
July 1, 1945 — June 30, 1946.	R. & M. No. 2050.	1*s*. (1*s*. 1½*d*.)
July 1, 1946 — December 31, 1946.	R. & M. No. 2150.	1*s*. 3*d*. (1*s*. 4½*d*.)
January 1, 1947 — June 30, 1947.	R. & M. No. 2250.	1*s*. 3*d*. (1*s*. 4½*d*.)
July, 1951.	R. & M. No. 2350.	1*s*. 9*d*. (1*s*. 10½*d*.)
January, 1954.	R. & M. No. 2450.	2*s*. (2*s*. 1½*d*.)
July, 1954.	R. & M. No. 2550.	2*s*. 6*d*. (2*s*. 7½*d*.)

Prices in brackets include postage

Obtainable from

HER MAJESTY'S STATIONERY OFFICE

York House, Kingsway, London, W.C.2; 423 Oxford Street, London, W.1 (Post Orders: P.O. Box 569, London, S.E.1); 13a Castle Street, Edinburgh 2; 39 King Street, Manchester 2; 2 Edmund Street, Birmingham 3; 109 St. Mary Street, Cardiff; Tower Lane, Bristol 1; 80 Chichester Street, Belfast, or through any bookseller

S.O. Code No. 23-2912